Astronomy & Astrophysics manuscript no. ms
(DOI: will be inserted by hand later)

The photospheric abundances of active binaries

II. Atmospheric parameters and abundance patterns for 6 single-lined RS CVn systems⋆

T. Morel[1], G. Micela[1], F. Favata[2], D. Katz[3], and I. Pillitteri[4]

[1] Istituto Nazionale di Astrofisica, Osservatorio Astronomico di Palermo G. S. Vaiana, Piazza del Parlamento 1, I-90134 Palermo, Italy
[2] Astrophysics Division - Research and Science Support Department of ESA, ESTEC, Postbus 299, NL-2200 AG Noordwijk, The Netherlands
[3] Observatoire de Paris, GEPI, Place Jules Janssen, F-92195 Meudon, France
[4] Dipartimento di Scienze Fisiche ed Astronomiche, Università di Palermo, Piazza del Parlamento 1, I-90134 Palermo, Italy

Received ?; accepted ?

Abstract. Photospheric parameters and abundances are presented for a sample of single-lined chromospherically active binaries from a differential LTE analysis of high-resolution spectra. Abundances have been derived for 13 chemical species, including several key elements such as Li, Mg, and Ca. Two methods have been used. The effective temperatures, surface gravities and microturbulent velocities were first derived from a fully self-consistent analysis of the spectra, whereby the temperature is determined from the excitation equilibrium of the Fe I lines. The second approach relies on temperatures derived from the $(B-V)$ colour index. These two methods give broadly consistent results for the stars in our sample, suggesting that the neutral iron lines are formed under conditions close to LTE. We discuss the reliability in the context of chromospherically active stars of various colour indices used as temperature indicators, and conclude that the $(V-R)$ and $(V-I)$ colours are likely to be significantly affected by activity processes. Irrespective of the method used, our results indicate that the X-ray active binaries studied are not as metal poor as previously claimed, but are at most mildly iron-depleted relative to the Sun ($-0.41 \lesssim$ [Fe/H] $\lesssim +0.11$). A significant overabundance of several chemical species is observed (e.g., the α-synthezised elements). These abundance patterns are discussed in relation to stellar activity.

Key words. Stars:fundamental parameters – stars:abundances – stars:individual: HD 10909, HD 72688, HD 83442, HD 101379, HD 113816, HD 118238, HD 119285, HD 124897

1. Introduction

The coronal abundances of active binaries have come under close scrutiny in recent years, thanks to several X-ray satellites such as *XMM-Newton* or *Chandra* (see Favata & Micela 2003 for a review). While these studies consistently yield a low coronal iron content, the abundance ratios determined for elements with strong X-ray lines (i.e., mainly Fe, Ni, O, Mg, Si, and Ca) appear not only discrepant with respect to the photospheric solar mix, but also significantly different from the values observed in the solar corona, where the abundances of elements with a low first ionization potential are enhanced compared to the solar photosphere (e.g., Audard et al. 2003).

A detailed comparison between coronal and photospheric abundances in active binaries would provide useful insights into the chemical fractionation processes that are likely to operate between the photosphere and the corona. Unfortunately, such a comparison is made difficult by the extreme paucity of photospheric abundance determinations for elements other than iron. Another issue is the heterogeneous nature of the abundance analyses performed to date, often resulting in conflicting results in the literature. Most studies of the iron abundance in active binaries have relied on temperatures derived from photometric indices (e.g., Randich, Gratton, & Pallavicini 1993), despite the fact that these stars are known to exhibit photometric anomalies related to their high level of activity (Giménez et al. 1991; Morale et al. 1996; Favata et al. 1997). The reliability of photometric colours as temperature indicators in active binaries and the possible impact on the resulting abundances needs therefore to be addressed. In the most extensive study to date, Randich et al. (1993) and Randich, Giampapa, & Pallavicini (1994) analyzed a total of 67 components in 54 binary systems by performing a spectral synthesis over a 25 Å-wide spectral domain encompassing the Li I λ6708 doublet. The surface gravities were estimated from the spectral type and the lumi-

Send offprint requests to: T. Morel, e-mail: morel@astropa.unipa.it

⋆ Based on observations collected at ESO (La Silla, Chile).

nosity class, or directly computed when radii and masses were known. The microturbulent velocity was calibrated on the luminosity class. The vast majority of these systems was found to be significantly iron-deficient with respect to the Sun ($-1.0 \lesssim$ [Fe/H] $\lesssim +0.2$, with a mean of -0.4). However, Fekel & Balachandran (1993) determined the iron abundance of some objects in this sample from a spectral synthesis of a similarly small spectral region, but with temperatures determined by fitting temperature-sensitive pairs of Fe I lines, obtaining abundances up to 0.5 dex higher. Ottmann, Pfeiffer, & Gehren (1998) determined temperatures from the wings of the Balmer lines and iron abundances from a set of Fe II lines for a small sample of RS CVn binaries. At variance with previous investigations, they find near-solar iron abundances. Abundances of key elements, such as O, Mg, etc., are only available for very few systems (Donati, Henry, & Hall 1995; Gehren, Ottmann, & Reetz 1999; Ottmann et al. 1998; Savanov & Berdyugina 1994).

To address the above issues we have started a project to derive in a self-consistent way photospheric parameters and metal abundances for a large sample of active binaries. In the first paper of this series (Katz et al. 2003 — hereafter Paper I), we have presented a detailed analysis of HD 113816 (IS Vir) and HD 119285 (V851 Cen), and critically discussed the applicability to active binaries of three methods commonly used in abundance determinations: (1) temperature and gravity derived from the excitation and ionization equilibria of the Fe lines, (2) temperature derived from colour indices and gravity from the ionization equilibrium of the Fe lines, and (3) temperature derived from colour indices and gravity from fitting the wings of collisionally-broadened lines. It was concluded that these methods gave for both stars broadly consistent results, although the $(V-I)$-based method gave too low a temperature. This also argued for small departures from LTE of the Fe I lines in the two stars studied. The iron content of HD 119285 was found to be 0.5 dex higher than the value derived by Randich et al. (1994). There was also some indication for a systematic overabundance of several key elements with respect to the solar pattern.

In the present paper we extend this study to 6 single-lined systems and examine their abundance patterns and evolutionary status. We re-analyze the two stars already discussed in Paper I (HD 113816 and HD 119285) because of significant differences between the 2 line lists; we also derive the abundances of 3 additional chemical species: Li, Cr, and Ba. In addition, we use our larger sample to re-examine in some more detail the reliability in the context of active binaries of various methods used in abundance analyses.

2. Observations and data reduction

Spectra of 28 active binary systems (18 SB1 and 10 SB2) were acquired in January 2000 at the ESO 1.52-m telescope (La Silla, Chile) with the fiber-fed, cross-dispersed echelle spectrograph FEROS in the object+sky configuration. The spectral range covered is 3600–9200 Å, with a resolving power of 48 000.

The program stars are drawn from a magnitude-limited subset ($V \lesssim 10$) of the catalogue of chromospherically active stars of Strassmeier et al. (1993). Since the curve-of-growth abundance analysis presented in the following is unapplicable to rapid rotators because of severe blending problems, here we restrict ourselves to studying 6 single-lined systems with a modest projected rotational velocity ($v \sin i \lesssim 10$ km s^{-1}). The other single-lined systems will be analized by means of other techniques (e.g., spectral synthesis), and will be, along with the spectroscopic binaries, the subject of future publications in this series. Some basic properties of the stars discussed in this paper are presented in Table 1. Our sample is made up of stars with very similar spectral types and is therefore highly homogeneous.

The data reduction (i.e., bias subtraction, flat-field correction, removal of scattered light, order extraction and merging, as well as wavelength calibration) was carried out during the observations.[1] Two to three consecutive exposures were generally obtained to allow a more robust continuum rectification and removal of cosmic ray events. Changes of physical origin in the spectral characteristics (e.g., because of flaring) are very unlikely to operate on the timescales considered (less than 1200 s), and no significant line-profile variations between consecutive exposures are indeed found. The journal of observations is presented in Table 1. The continuum normalization was achieved in 2 steps. A synthetic Kurucz model atmosphere (Kurucz 1993) calculated for an initial guess of the stellar spectral type and luminosity class (with solar metallicity) was first used to roughly determine the line-free regions, which were then fitted by low-degree polynomials (the spectra have been continuum-normalized by segments of 200 to 400 Å). More accurate estimates of the atmospheric parameters were obtained after the spectral analysis detailed below was carried out, and this procedure was re-iterated.

3. Line selection and atomic data calibration

In Paper I unblended lines were selected from inspection of a synthetic spectrum computed with Piskunov's SYNTH program using atomic parameters from the VALD database (Piskunov et al. 1995; Kupka et al. 1999, 2000) and a Kurucz model atmosphere. Here we use instead a high-resolution spectrum of the K1.5 III star Arcturus (Hinkle et al. 2000). This star is well-matched in terms of spectral type to the stars under consideration (see Table 1). No attempts was made to select lines blueward of 5500 Å because of the difficulty in defining the continuum in this region. Special care was taken to select a set of neutral iron lines spanning a wide range in excitation potential and strength. Low-excitation neutral lines (except for iron) were discarded, as they are bound to be the most affected by NLTE effects. We followed the prescription of Ruland et al. (1980), by only retaining transitions arising from levels less than 4.4 eV below the ionization limit. For the few remaining lines with detailed calculations, the NLTE corrections appear modest: they range from $\Delta\epsilon = \log(\epsilon)_{\rm NLTE} - \log(\epsilon)_{\rm LTE} = -0.09$ to -0.03 dex for Na I λ6154, from $+0.05$ to $+0.06$ dex for Mg I λ5711 (Gratton et al. 1999), and from $+0.01$ to $+0.09$ dex for

[1] With the *"FEROS Data Reduction Software"* available at: `http://www.ls.eso.org/lasilla/Telescopes/2p2T/E1p5M/FEROS/offline.`

Table 1. Spectral type, maximum V magnitude, projected rotational velocity, rotational and orbital periods, number of consecutive exposures obtained, mean heliocentric Julian date of the observations, and typical S/N ratio at 6700 Å in the combined spectrum.

Name	Spectral type[a]	V^a (mag)	$v \sin i^b$ (km s^{-1})	$P_{\rm rot}{}^c$ (d)	$P_{\rm orb}{}^c$ (d)	N	(HJD–2,451,500)	S/N
HD 10909 (UV For)	K0 IV	8.10	2.7	64.1	30.11	2	51.59	150
HD 72688 (VX Pyx)	K0 III	6.37	7.4	19.34	45.13	1	51.80	250
HD 83442 (IN Vel)	K2 IIIp	9.10	7.5	54.95	52.27	2	51.82	140
HD 113816 (IS Vir)	K2 IV-III	8.37	5.9	24.10	23.65	3	53.79	180
HD 118238 (V764 Cen)	K2 IIIp	9.06	11	22.62	22.74	2	51.86	140
HD 119285 (V851 Cen)	K2 IV-III	7.69	6.5	12.05	11.99	1	53.84	200

[a]: From Strassmeier et al. (1993).
[b]: Primarily from Fekel (1997) and de Medeiros & Mayor (1999); from Strassmeier et al. (1993) when not available. For HD 118238, estimate based on the spectral synthesis of the Li I λ6708 doublet (Sect 5.3).
[c]: From Strassmeier et al. (1993), except for HD 10909 and HD 113816 (Fekel et al. 2001, 2002).

the Ca lines (Drake 1991). These corrections have been applied to the abundances derived here.

All gf-values have been calibrated on the Sun, i.e., a high S/N moonlight spectrum acquired with the same instrumental configuration as the target stars was used in conjunction with a LTE plane-parallel Kurucz solar model (with $T_{\rm eff}$ = 5777 K, $\log g$ = 4.44 cm s^{-2}, and a depth-independent microturbulent velocity ξ = 1.0 km s^{-1}; Cox 2000) to carry out exactly the same abundance analysis as detailed below for the active binaries. The oscillator strengths were then adjusted until Kurucz's solar abundances were reproduced. For O I λ6300.304, we corrected the solar equivalent width (EW) for the contribution of Ni I λ6300.339 (Allende Prieto, Lambert, & Asplund 2001). In order to be consistent with Kurucz models and opacities, we adopt $\log \epsilon_{\odot}$(Fe)=7.67. As the analysis performed here is purely differential with respect to the Sun, using the meteoritic value instead ($\log \epsilon_{\odot}$[Fe]=7.50; Grevesse & Sauval 1998) would have no consequence on our results. All lines initially selected (with the exception of O I λ6300) which were too weak ($EW \lesssim 10$ mÅ), affected by telluric features, or too distorded to have their EWs reliably measured in the solar spectrum were discarded. The derived oscillator strengths were compared with previous estimates in the literature (Edvardsson et al. 1993; Feltzing & Gonzalez 2001; Kurucz & Bell 1995; Neuforge-Verheecke & Magain 1997: Reddy et al. 2003), and 11 lines with a suspicious gf-value were rejected. These exhibited (1) a discrepancy greater than 0.5 dex when the only source of comparison was Kurucz & Bell (1995) or (2) a systematic shift greater than 0.1 dex with other values in the literature. The final line list and a discussion regarding the atomic data can be found in the Appendix.

4. Methodology

Method 1: The photospheric parameters ($T_{\rm eff}$, $\log g$, and ξ) and metal abundances were first determined from a self-consistent analysis of the spectra by using the measured EWs and the latest generation of Kurucz LTE plane-parallel atmospheric models computed with the ATLAS9 code (Kurucz 1993) as input for the MOOG software originally developed by Sneden (1973). We use models with a length of the convective cell over the pressure scale height, $\alpha = l/H_{\rm p} = 0.5$ (e.g., Fuhrmann, Axer, & Gehren 1993), and without overshooting. These choices have a negligible impact on our derived abundances (less than 0.02 dex). The model parameters ($T_{\rm eff}$, $\log g$, ξ, [Fe/H], and [α/Fe]) are iteratively modified until: (1) the Fe I abundances exhibit no trend with excitation potential or reduced equivalent width (the EW divided by the wavelength of the transition), (2) the abundances derived from the Fe I and Fe II lines are identical, and (3) the Fe and α-element abundances are consistent with the input values. As will be shown in the following, most of our stars exhibit a noticeable enhancement of the electron-donor elements Mg, Si, Ca, and Ti. When appropriate, we therefore used atmospheric models with [α/Fe]=0.2 and 0.4 to account for the increase in the continuous H^- opacity.

A concern is that departures from LTE for the low-excitation Fe I lines would bias our determination of the excitation temperature and ultimately abundances. For K-type subgiants, the models of Thévenin & Idiard (1999) and Gratton et al. (1999) suggest NLTE corrections of the order of $\Delta\epsilon \approx +0.05$ dex. Test calculations for HD 10909 indicate that artificially decreasing the abundance of the Fe I lines with a first excitation potential, χ, below 3.5 eV (Ruland et al. 1980) by this amount would lead to an increase of 85 K and 0.25 dex in $T_{\rm eff}$ and $\log g$, respectively. The resulting mean iron abundance would *increase* by about 0.06 dex *after* fulfilment of the excitation and ionization equilibria of the Fe lines. Only [Ba/Fe] would be significantly affected (+0.11 dex), while the changes would be less than 0.05 dex for the other elements.

Method 2: Although the method detailed above appears robust against NLTE effects at the anticipated level, we further assessed the reliability of our results by carrying out the same analysis, but after excluding the Fe I lines with $\chi < 3.5$ eV. The effective temperature was in this case determined from the empirical $T_{\rm eff}$-colour calibrations for F0–K5 giants of Alonso, Arribas, & Martínez-Roger (1999, 2001) using the iron abundance obtained by Method 1. Table 2 lists the photometric properties of our program stars, along with the temperatures derived from the $(B-V)$, $(V-R)$ and $(V-I)$ colours. We use

in the following the temperature determined from the $(B-V)$ index, as being a more reliable indicator of the stellar effective temperature (Paper I). The values derived from the $(V-R)$ and $(V-I)$ data will be primarily used to assess the reliability of colour temperatures in chromospherically active stars. We do not attempt to use the Balmer lines to constrain the temperature, as this method is not well-suited for the coolest stars in our sample (e.g., Barklem et al. 2002).

The uncertainties on the atmospheric parameters arise mainly from the errors inherent to the determination of the excitation and ionization equilibria of the iron lines ($T_{\rm eff}$ and $\log g$), or from constraining the abundances given by the Fe I lines to be independent of the reduced equivalent width (ξ). To estimate the uncertainty on $T_{\rm eff}$, for instance, we considered the $1\,\sigma$ statistical error on the slope of the relation between the Fe I abundances and the excitation potentials. The 3 parameters of the atmospheric models were subsequently varied by the relevant uncertainty, and the effect on the mean abundance of each element derived. Other sources of uncertainties include the line-to-line scatter in the abundance determinations and the errors in the EW measurements (the latter estimated on a star-to-star basis). These 5 individual "$1\,\sigma$ errors" were finally quadratically summed, ignoring any covariance terms. Following standard practice, this error budget does not take into account systematic errors. However, the strictly differential nature of our analysis minimizes many of them (e.g., inaccurate atomic data). The abundances of some elements (Na, Mg, and Ba) were derived from a single, strong line lying on the flat portion of the curve of growth, and should therefore be treated with some caution. As in Paper I, we assume for the colour temperatures an uncertainty of 150 K ($B-V$) and 100 K ($V-R$ and $V-I$). These figures take into account typical photometric uncertainties, internal errors in the calibration, and systematic differences with other empirical relations (Alonso et al. 1999). For the metallicity-dependent $T_{\rm eff}$-$(B-V)$ calibration, the uncertainties on [Fe/H] were also considered.

The EWs (see Table A.1) were measured with the task *splot* implemented in the IRAF[2] software, assuming Gaussian profiles. Only lines with a satisfactory fit were retained. For the most rapid rotators, more severely affected by blending problems, this resulted in a drastic reduction in the number of lines used. Measurements performed on consecutive exposures suggest typical internal errors of the order of 3 mÅ ($\approx$ 4%) for weak or moderately strong lines ($EW \lesssim 100$ mÅ), while this uncertainty is typically 2 mÅ ($\approx$ 1%) for stronger lines. For HD 113816 and HD 119285, an excellent agreement was found for the EWs of the 44 transitions in common with Paper I, despite a rectification procedure and measurements carried out completely independently.

Although any abundance analysis should preferentially rely on weak lines that both lie on the linear part of the curve of growth and are insensitive to the uncertain treatment of collisional broadening, this is difficult to achieve in practice for such cool stars with moderate rotational velocities because of blending problems. As many damping constants are poorly known, all the lines that may have been significantly van der Walls broadened (i.e., those with $\log[EW/\lambda] > -4.55$) were discarded from the analysis. This damping process is a minor contributor to the EWs of the remaining transitions, and was accounted for by the Unsöld approximation in the computation of MOOG theoretical curves of growth (Unsöld 1955). Calculations including empirical enhancement factors (Simmons & Blackwell 1982) would give very similar results ($\Delta T_{\rm eff} \lesssim 30$ K, $\Delta \log g \lesssim 0.15$ dex, Δ[Fe/H] $\lesssim 0.03$ dex, Δ[M/Fe] $\lesssim 0.05$ dex). As shown in Paper I, the use of strong Fe I lines (with EWs up to 160 mÅ) is not thought to substantially affect our results. The selected transitions of the odd-Z elements (Sc, Co, and Ba) are not significantly broadened by hyperfine structure (Mashonkina et al. 2003; Prochaska et al. 2000; Reddy et al. 2003). The Sc and Co lines are weak in our spectra. Atomic lines affected by telluric features were also discarded (we used the telluric atlas of Hinkle et al. 2000). Between 37 and 80 lines were used in total for each star (among which between 18 and 47 iron lines).

5. Results and discussion

5.1. Abundances and atmospheric parameters

Table 3 gives the atmospheric parameters and abundances determined from Methods 1 and 2. Compared to Paper I, the iron abundances of HD 113816 and HD 119285 are lower by 0.15 and 0.10 dex, respectively. The temperatures and surface gravities agree to within 70 K and 0.20 dex, respectively. The abundance ratios of the other chemical elements (prior to our NLTE corrections which were not applied in Paper I) are within the range of the expected uncertainties, with no systematic trends. In some cases (e.g., Mg), the differences are largely due to the different atomic data used.

The two methods used yield in some cases significantly different values for the effective temperatures and surface gravities (Table 3). The differences may reach up to 110 K for $T_{\rm eff}$ and up to 0.35 dex for $\log g$. However, this only has a noticeable impact on the abundance of barium (0.13 dex). For the other elements (including Fe), the results given by the 2 methods are not significantly different (0.08 dex at most).

Our results regarding the atmospheric parameters and iron content of these active binaries appear at variance with previous studies and suggest that these systems may not be as iron-depleted as previously claimed (Randich et al. 1993, 1994). With the exception of HD 10909, we derive systematically higher effective temperatures and iron abundances (see Table 4). The surface gravities are also significantly different. In the most extreme case (HD 113816), we derive a temperature higher by 250 K, a gravity lower by 1.25 dex and an iron content higher by almost 0.8 dex than Randich et al. (1994). These large discrepancies in the iron abundances are unlikely to be solely accounted for by differences in the temperature scale; differences in the gravity and microturbulent velocity (which were often simply calibrated on the spectral type and luminosity class) are also likely to play a role.

[2] IRAF is distributed by the National Optical Astronomy Observatories, operated by the Association of Universities for Research in Astronomy, Inc., under cooperative agreement with the National Science Foundation.

Table 2. Distance, extinction in the V band, colour excesses because of interstellar extinction, dereddened colours, and effective temperatures. The iron abundances quoted in this table (from Method 1) were used to derive the effective temperatures from the $(B-V)$ and $(V-R)$ colours (see Alonso et al. 1999).

	HD 10909	HD 72688	HD 83442	HD 113816	HD 118238	HD 119285
d (pc)[a]	130	131	286	300	760	76
$A(V)$ (mag)[b]	0.100	0.078	0.220	0.174	0.294	0.115
$E(B-V)$ (mag)[c]	0.030	0.024	0.067	0.053	0.090	0.035
$E(V-R)_c$ (mag)[c]	0.019	0.015	0.041	0.033	0.055	0.022
$E(V-R)$ (mag)[c]	0.025	0.019	0.055	0.043	0.073	0.029
$E(V-I)_c$ (mag)[c]	0.040	0.031	0.089	0.070	0.118	0.046
$E(V-I)$ (mag)[c]	0.052	0.041	0.115	0.091	0.153	0.060
$(B-V)_0$ (mag)	0.930	0.926	1.103	1.057	1.170	1.045
$(V-R)_0$ (mag)	0.755	0.692	0.862	0.887	0.911	0.860
$(V-I)_0$ (mag)	1.285	1.168	1.454	1.379	1.545	1.483
Reference[d]	S93	C	S93	HIPP($B-V$), S93	S93	C
[Fe/H]	–0.41	+0.11	+0.02	–0.11	–0.12	–0.23
$T_{colour}(B-V)$ (K)	4831±150	4989±150	4616±150	4668±150	4470±150	4662±150
$T_{colour}(V-R)$ (K)	4741±100	4962±100	4510±100	4445±100	4394±100	4495±100
$T_{colour}(V-I)$ (K)	4730±100	4939±100	4469±100	4580±100	4347±100	4429±100
T_{exc} (K)[e]	4830±87	5045±62	4715±87	4700±77	4575±119	4770±77

[a]: Adopted distance for the determination of the interstellar extinction, derived from *Hipparcos* data (ESA 1997) for the stars with accurate trigonometric parallaxes (see Table 10). Distance for HD 118238 from Strassmeier et al. (1993).
[b]: Determined from the empirical model of galactic interstellar extinction of Arenou, Grenon, & Gómez (1992). The stellar galactic coordinates are quoted in Table 10.
[c]: Conversion factors from Cardelli, Clayton, & Mathis (1989) and Schlegel, Finkbeiner, & Davis (1998).
[d]: References for the photometric data. S93: Strassmeier et al. (1993) and references therein; HIPP: *Hipparcos* data (ESA 1997); C: Cutispoto, Messina, & Rodonò (2001). The colours in the Cousins system, $(V-R)_c$ and $(V-I)_c$, were converted into $(V-R)$ and $(V-I)$ Johnson colours following Bessel (1979).
[e]: Temperatures determined from the excitation equilibrium of the Fe I lines (see text).

The oxygen abundance could be reliably measured from O I λ6300 for 2 stars in our sample (HD 10909 and HD 113816), but inconsistencies are found with the results given by the O I triplet at 7774 Å. For HD 113816, for instance, we obtain [O/Fe] = −0.22 and +1.19 dex for O I λ6300 and the near-IR O I triplet, respectively. Such a difference is too large to be accounted for by granulation effects (Nissen et al. 2002) or by departures from LTE ($\Delta\epsilon = -0.13$ to -0.05 dex; Gratton et al. 1999). A much hotter oxygen line-forming region (perhaps because of chromospheric heating) would help reducing the discrepancy because of the inverse sensitivity of these spectral features to the temperature (e.g., Cavallo, Pilachowski, & Rebolo 1997). Although this is not clearly borne out by our exploratory calculations (see below), it remains to be fully worked out theoretically. Alternative explanations include an unusually strong ultraviolet radiation field (Vilhu, Gustafsson, & Edvardsson 1987). In view of these problems, the oxygen abundance is not discussed in the following (the EWs of the oxygen features are given in Table A.1 for completeness).

A striking feature of the abundance patterns, irrespective of the method used, is the overabundance of most elements with respect to iron (Fig. 1).[3] Figure 2 shows the abundance ratios derived by both methods as a function of [Fe/H]. Only the iron-peak elements Co and Ni present abundances that are broadly consistent with the solar values, with a hint that nickel is slightly depleted. The abundance ratio of the neutron-capture element Ba exhibits a large spread for a given [Fe/H] value, as generally found for field dwarfs (e.g., Reddy et al. 2003). There is a clear indication for an increasing overabundance of the α-elements (defined as the mean of the Mg, Si, Ca, and Ti abundances) with decreasing [Fe/H].

To assess the robustness of our results we carried out the same analysis on a high-resolution spectrum of Arcturus (Hinkle et al. 2000). We used the same line list and calibrated atomic data as for the active binaries. Our results are given in Table 5 where they are compared with previous estimates in the literature. Our effective temperature and surface gravity are at the lower end of the previous estimates, but are very similar to the values of Mäckle et al. (1975). There is no evidence that our analysis systematically yields spuriously high abundance ratios. Compared to the mean values in the literature, the abundances of the elements heavier than Na differ on average by only 0.04 dex. Once again, we find a discrepancy between the oxygen abundances given by O I λ6300 and the near-IR triplet (0.6 dex) which is too large to be simply accounted for by NLTE effects (Gratton et al. 1999; Takeda 2003). This suggests that the discrepancy observed in the active binaries may not be entirely attributed to activity, but also

[3] It has to be kept in mind that NLTE corrections were applied to Na, Mg and Ca, but not to the other elements (Sect. 3). There is therefore a systematic, albeit small, zero-point offset between [Na/Fe], [Mg/Fe], [Ca/Fe] and the other abundance ratios.

Table 3. Mean values of the atmospheric parameters and abundances as determined from Methods 1 and 2 (<>). The corresponding 1 σ uncertainties and the number of lines included in the abundance analysis (N) are also indicated. The abundances of Na, Mg and Ca have been corrected for departures from LTE (see text). The lithium abundances are given in Table 9. Blanks indicate that no EWs for the element in question could be reliably measured. We use the usual notation: [A/B]=log $[\mathcal{N}(A)/\mathcal{N}(B)]_\star$−log $[\mathcal{N}(A)/\mathcal{N}(B)]_\odot$.

	HD 10909 (UV For)				HD 72688 (VX Pyx)				HD 83442 (IN Vel)			
	Method 1		Method 2		Method 1		Method 2		Method 1		Method 2	
	N	<>	N	<>	N	<>	N	<>	N	<>	N	<>
$T_{\rm eff}$ (K)		4830± 87		4831±150		5045±62		4989±150		4715±87		4616±150
log g (cm s^{-2})		2.90±0.13		2.90±0.13		2.77±0.10		2.58±0.09		2.75±0.13		2.40±0.11
ξ (km s^{-1})		1.48±0.09		1.48±0.08		1.62±0.06		1.62±0.07		1.89±0.09		1.89±0.10
[Fe/H][a]	47	–0.41±0.09	37	–0.41±0.12	42	0.11±0.07	36	0.07±0.12	41	0.02±0.10	35	–0.05±0.14
[Na/Fe]	1	0.27±0.06	1	0.27±0.10	1	0.45±0.05	1	0.46±0.09	1	0.47±0.06	1	0.48±0.11
[Mg/Fe]	1	0.42±0.03	1	0.42±0.08	1	–0.04±0.04	1	–0.02±0.09	1	0.13±0.04	1	0.16±0.10
[Al/Fe]	2	0.42±0.04	2	0.42±0.07	2	0.18±0.06	2	0.20±0.08	2	0.39±0.10	2	0.41±0.14
[Si/Fe]	8	0.24±0.06	8	0.24±0.08	4	0.10±0.06	4	0.12±0.07	7	0.14±0.15	7	0.19±0.15
[Ca/Fe]	3	0.36±0.07	3	0.36±0.15	3	0.08±0.08	3	0.08±0.15	3	0.24±0.06	3	0.22±0.15
[Sc/Fe]	1	0.17±0.13	1	0.17±0.19								
[Ti/Fe]	1	0.35±0.08	1	0.35±0.13	1	0.16±0.09	1	0.16±0.14	1	0.19±0.07	1	0.17±0.13
[Cr/Fe]	4	0.07±0.10	4	0.07±0.14	4	0.00±0.08	4	–0.01±0.14	2	0.15±0.11	2	0.13±0.17
[Co/Fe]	1	0.18±0.09	1	0.18±0.15	1	0.01±0.10	1	0.00±0.15	1	0.10±0.09	1	0.08±0.15
[Ni/Fe]	10	–0.02±0.08	10	–0.02±0.13	10	–0.06±0.08	10	–0.06±0.14	9	–0.04±0.11	9	–0.04±0.15
[Ba/Fe]	1	–0.05±0.11	1	–0.05±0.26	1	0.15±0.08	1	0.11±0.24	1	0.10±0.13	1	0.00±0.29

	HD 113816 (IS Vir)				HD 118238 (V764 Cen)				HD 119285 (V851 Cen)			
	Method 1		Method 2		Method 1		Method 2		Method 1		Method 2	
	N	<>	N	<>	N	<>	N	<>	N	<>	N	<>
$T_{\rm eff}$ (K)		4700±77		4668±150		4575±119		4470±150		4770±77		4662±150
log g (cm s^{-2})		2.45±0.21		2.30±0.15		2.40±0.28		2.08±0.28		3.10±0.19		2.80±0.21
ξ (km s^{-1})		1.79±0.08		1.79±0.07		2.78±0.19		2.78±0.21		1.71±0.07		1.74±0.09
[Fe/H][a]	46	–0.11±0.09	40	–0.14±0.13	20	–0.12±0.13	18	–0.20±0.16	44	–0.23±0.10	36	–0.31±0.13
[Na/Fe]	1	0.35±0.06	1	0.36±0.11	1	0.41±0.25	1	0.40±0.28	1	0.46±0.05	1	0.47±0.11
[Mg/Fe]	1	0.11±0.03	1	0.13±0.09					1	0.28±0.03	1	0.31±0.08
[Al/Fe]	2	0.19±0.06	2	0.21±0.10	2	0.51±0.25	2	0.53±0.29	2	0.48±0.05	2	0.51±0.12
[Si/Fe]	4	0.08±0.11	4	0.09±0.11	4	0.34±0.18	4	0.39±0.21	4	0.18±0.09	4	0.22±0.11
[Ca/Fe]	3	0.25±0.09	3	0.25±0.16	2	0.03±0.15	2	0.01±0.21	3	0.35±0.08	3	0.34±0.17
[Sc/Fe]	1	–0.03±0.13	1	–0.06±0.19					1	0.16±0.16	1	0.09±0.21
[Ti/Fe]	1	0.16±0.08	1	0.16±0.14	1	0.36±0.16	1	0.34±0.19	1	0.33±0.08	1	0.32±0.14
[Cr/Fe]	3	0.12±0.08	3	0.12±0.15	1	0.09±0.32	1	0.07±0.35	3	0.25±0.15	3	0.24±0.20
[Co/Fe]	1	0.00±0.08	1	–0.01±0.14	1	0.11±0.27	1	0.09±0.29	1	0.00±0.10	1	–0.03±0.14
[Ni/Fe]	9	–0.13±0.10	9	–0.13±0.14	6	–0.14±0.22	6	–0.15±0.25	9	–0.07±0.10	9	–0.07±0.15
[Ba/Fe]	1	0.34±0.11	1	0.31±0.26	1	–0.29±0.28	1	–0.42±0.37	1	0.18±0.14	1	0.07±0.29

[a]: Mean of the values for Fe I and Fe II.

Table 4. Comparison with previous studies.

	Fekel & Balachandran (1993)			Randich et al. (1993, 1994)			This study[a]		
Name	$T_{\rm eff}$ (K)	log g (cm s^{-2})	[Fe/H]	$T_{\rm eff}$ (K)	log g (cm s^{-2})	[Fe/H]	$T_{\rm eff}$ (K)	log g (cm s^{-2})	[Fe/H]
HD 10909 (UV For)				4900	3.3	–0.3	4830±87	2.90±0.13	–0.41±0.09
HD 72688 (VX Pyx)	4900	3.0	–0.07[b]	4900	2.5	–0.3	5045±62	2.77±0.10	0.11±0.07
HD 83442 (IN Vel)				4400	2.4	–0.4	4715±87	2.75±0.13	0.02±0.10
HD 113816 (IS Vir)				4450	3.7	–0.9	4700±77	2.45±0.21	–0.11±0.09
HD 119285 (V851 Cen)				4650	3.6	–0.6	4770±77	3.10±0.19	–0.23±0.10

[a] Values derived from Method 1.
[b] Value rescaled to our adopted solar iron abundance (log $\epsilon_\odot$[Fe]=7.67).

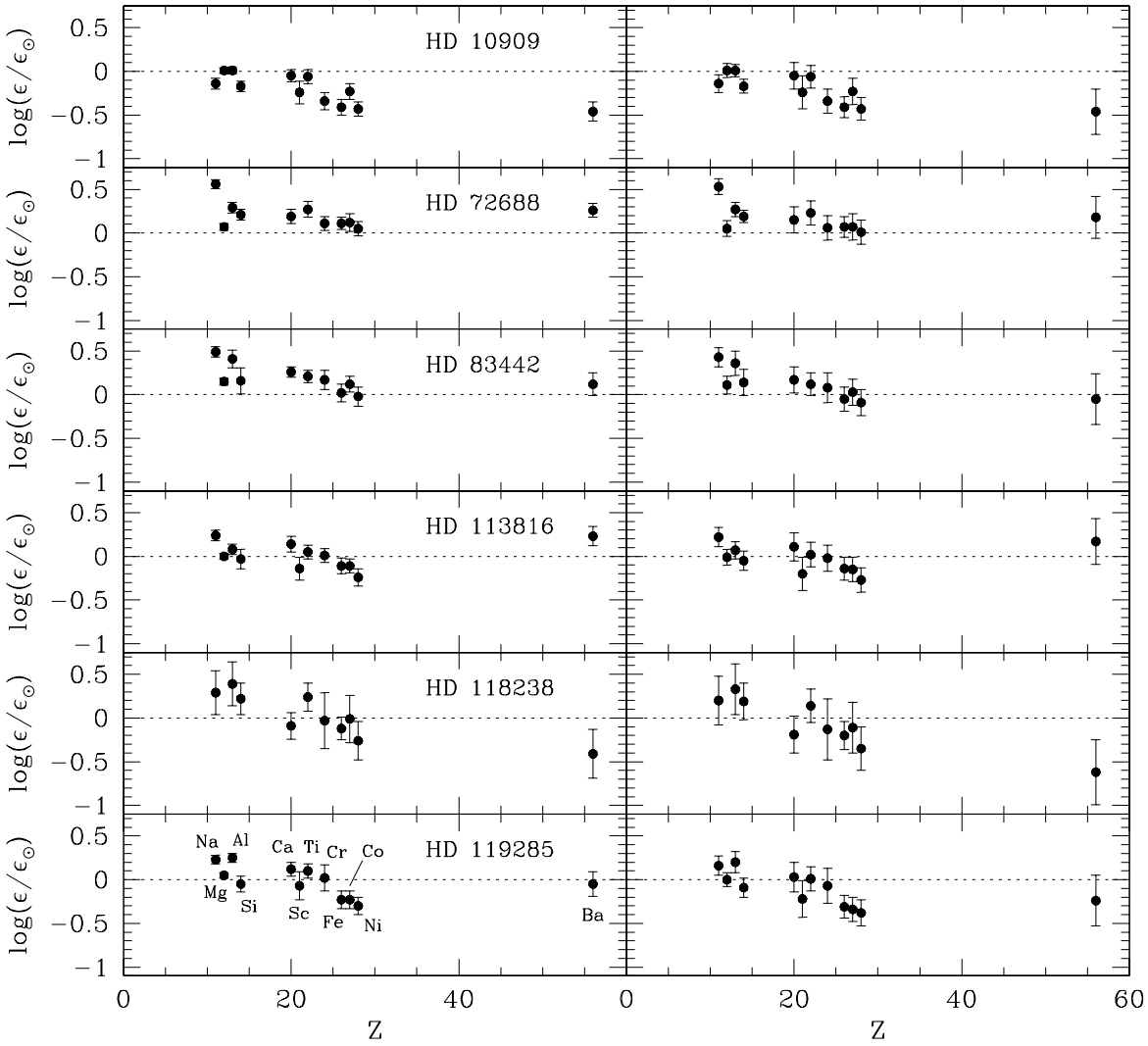

Fig. 1. Abundance patterns for the stars in our sample, determined from Method 1 (*left-hand panels*) and Method 2 (*right-hand panels*).

to other physical phenomena and/or caveats in the atmospheric models. Inconsistencies between these two oxygen abundance indicators in metal-poor stars is a long-standing, but still unresolved issue (e.g., Fulbright & Johnson 2003).

We now turn to examine the potential importance of chromospheric heating in inducing the overabundances observed. To this end, we follow the method of McWilliam et al. (1995), by merging the empirical chromospheric model of the K0 giant Pollux determined by Kelch et al. (1978) with our derived photospheric model for HD 10909. This modifies the temperature structure of the Kurucz model in two ways: (1) a reversal of the temperature gradient in the uppermost photospheric layers corresponding to column mass densities, $m < 0.30$ g cm^{-2}. The temperature at this point (which defines the onset of the chromosphere), $T_{\rm min}$, is set to $T_{\rm min} = 0.788 \times T_{\rm eff} = 3805$ K; (2) an overall heating (up to 190 K) of the upper photosphere between $m = 0.30$ and 14 g cm^{-2}. The temperatures of the Kurucz and empirical models are taken to be identical at $m = 14$ g cm^{-2}. The temperature-mass density relation of the merged model was interpolated between this point and the temperature minimum. The electronic density was calculated following Mihalas (1978). We also experimented with a more prominent chromospheric component, perhaps more akin to RS CVn binaries (Lanzafame, Busà, & Rodonò 2000). In this case, $T_{\rm min} = 0.870 \times T_{\rm eff} = 4200$ K and the temperature at the outermost layer of the Kurucz model is set to 5500 K (instead of 5100 K). The temperature structure of the 2 atmospheric models with an added chromospheric component is shown in Fig. 3. Determining an empirical model on a star-to-star basis (e.g., from fitting the chromospheric emission component of optical lines) would be obviously preferable, but is beyond the scope of this paper. We used these 2 atmospheric models to perform on the EWs determined for HD 10909 the same spectral analysis as described previously, varying $T_{\rm eff}$, $\log g$ and ξ until convergence. The chromospheric component was rescaled during this procedure, with $T_{\rm min}/T_{\rm eff}$ held constant and the temperature at the top of the model chromosphere decreased by the same amount as the effective temperature. The differences with

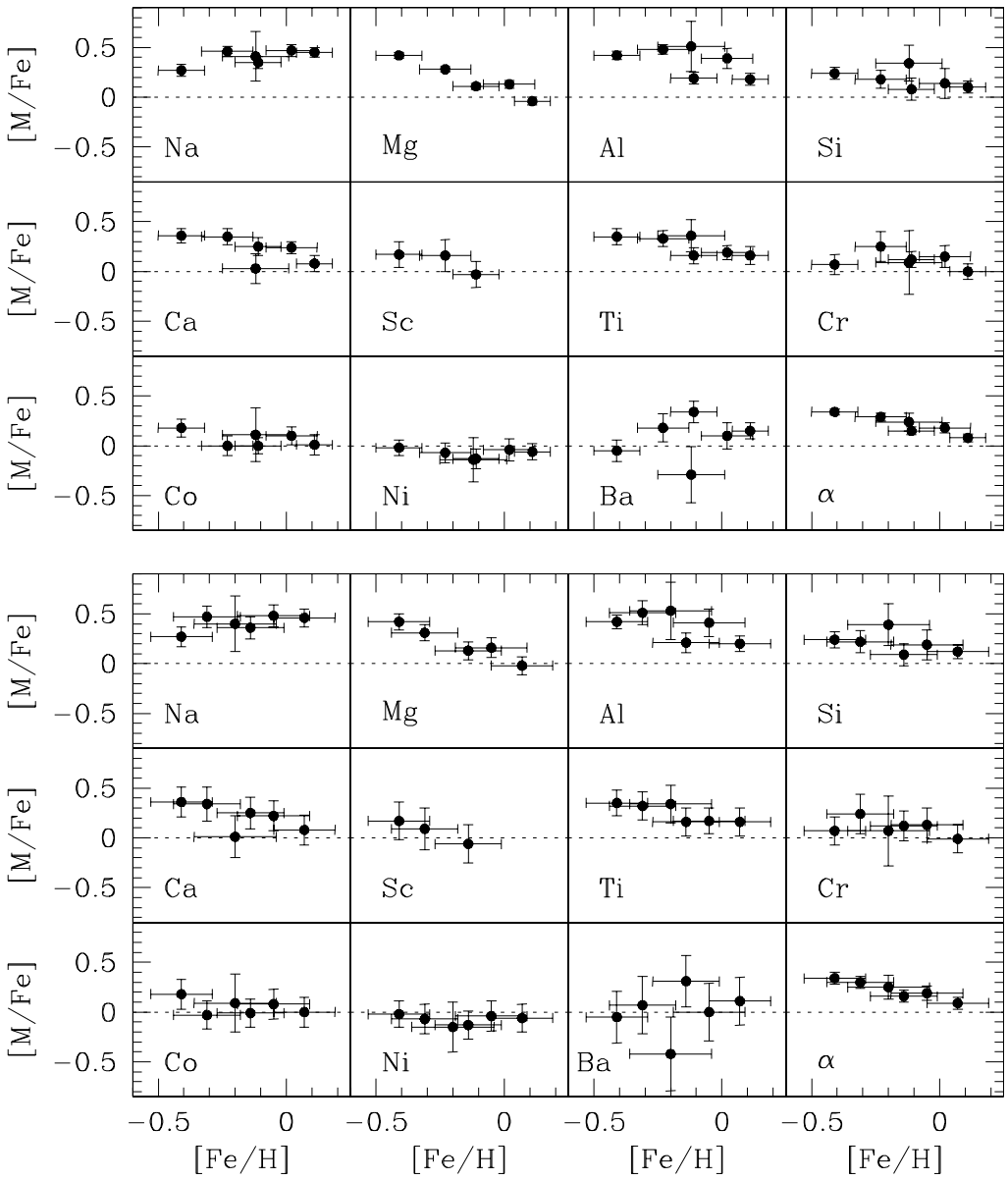

Fig. 2. Abundance ratios as a function of [Fe/H] for Method 1 (*top*) and Method 2 (*bottom*). We define a mean abundance ratio of the α-synthezised elements, [α/Fe], as the unweighted mean of the Mg, Si, Ca, and Ti abundances.

the results using the Kurucz models are presented in Table 6. Strong lines are found to be most affected by the inclusion of a chromosphere, as expected for lines formed in comparatively higher photospheric layers. The strong Fe I lines yield much higher abundances (up to 1.0 dex). As a result, requiring the iron abundance to be independent of the line strength leads to a strong increase of the microturbulent velocity. The overall heating induced by the chromospheric component needs to be compensated by an "incipient" phototospheric model with a much lower effective temperature (up to 360 K). Achieving ionization equilibrium of the Fe lines also requires a dramatically lower gravity, with differences reaching up to 1.1 dex for the model with $T_{\rm min}/T_{\rm eff}$ = 0.870. The fair agreement between our surface gravities and values derived from evolutionary tracks (Fig. 13) suggests that the effect of the chromosphere on the photospheric temperature structure may be less severe in reality than assumed by this model. In summary, assuming that the atmospheres of chromospherically active stars can be described by a Kurucz photospheric model leads to an *overestimation* of both the effective temperature and surface gravity. An overall heating of the upper photospheric layers because of chromospheric activity has a limited impact on the abundance ratios (except for Ba) and does not appear to systematically yield higher values (Table 6). The impact of a chromosphere on our abundance analysis is likely to be largely due to differences in the temperature structure of the upper photosphere where the LTE approximation is nearly valid. However, because this assumption of LTE breaks down in the low-density, high-temperature chromospheric regions, we warn the reader of the crudeness of these pilot calculations.

Table 5. Comparison between our results for Arcturus and previous estimates in the literature.

		References					
	This study[a]	(1)	(2)	(3)	(4)	(5)	(6)
$T_{\rm eff}$ (K)	4205	4260	4490	4350	4330	4300	
log g (cm s^{-2})	1.05	0.90	2.01	1.8	1.5	1.50	
ξ (km s^{-1})	1.59	1.8	1.8		1.5	1.7	
[Fe/H]	–0.72	–0.70	–0.56	–0.51	–0.38	–0.5	–0.5
[O/Fe] (6300)	0.17		0.40	0.26		0.4	0.40
[O/Fe] (7774)	0.76					0.4	
[Na/Fe]	0.26	0.25				0.3	0.20
[Mg/Fe]	0.56	0.50			0.24	0.4	0.40
[Al/Fe]	0.44	0.50				0.4	
[Si/Fe]	0.46	0.35			0.19	0.4	0.30
[Ca/Fe]	0.24	0.25			0.08	0.3	0.20
[Sc/Fe]	0.09	0.05				0.2	0.20
[Ti/Fe]	0.25	0.30			0.22	0.3	0.25
[Cr/Fe]	–0.02	0.05				0.0	
[Co/Fe]	0.33	0.10					
[Ni/Fe]	0.03	0.00			0.11	0.0	0.10
[Ba/Fe]	–0.27	–0.25					

[a]: For comparison purposes, no NLTE corrections have been applied to our results.
Key to references: (1) Mäckle et al. (1975); (2) Lambert & Ries (1981); (3) Kjærgaard et al. (1982); (4) Gratton & Sneden (1987); (5) Peterson, Dalle Ore, & Kurucz (1993); (6) Donati et al. (1995).

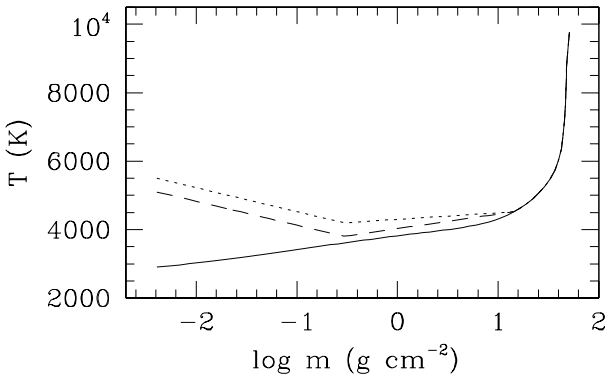

Fig. 3. Temperature structures for HD 10909 of the adopted Kurucz model (*solid*) and the 2 empirical models with an added chromospheric component (*dashed* and *dotted* line for $T_{\rm min}/T_{\rm eff}$ = 0.788 and 0.870, respectively).

To investigate further the effect of stellar activity, we looked for a correlation between the abundance ratios and the Ca II H+K emission-line fluxes (see Fig. 4) calculated following Linsky et al. (1979). The relative fluxes in the Ca II lines were first calculated by integrating the unnormalized spectra in the wavelength domain $\Delta\lambda(\rm K_1) = \lambda(\rm K_{1V}) - \lambda(\rm K_{1R})$ and $\Delta\lambda(\rm H_1) = \lambda(\rm H_{1V}) - \lambda(\rm H_{1R})$ (see Strassmeier et al. 1990 for definitions), and then dividing these values by the corresponding flux in the 3925–3975 Å bandpass, f_{50}. All measurements are performed from the zero-flux level. These relative fluxes, f, are converted into absolute surface fluxes, $\mathcal{F}$, using (the subscripts refer either to the K or to the H feature):

$$\mathcal{F}_{\rm K/H} = 50\,\frac{f_{\rm K/H}}{f_{50}}\,\mathcal{F}_{50} \qquad (1)$$

Table 6. Effect of chromospheric heating on the atmospheric parameters and abundances of HD 10909. For each quantity X, the results are given in the form: $\Delta X = X$(photosphere)$-X$(photosphere+chromosphere). The results for the model without a chromospheric component (Method 1) are given in Table 3.

ΔX	$T_{\rm min}/T_{\rm eff}$	
	0.788	0.870
$\Delta T_{\rm eff}$ (K)	200	360
Δlog g (cm s^{-2})	0.35	1.10
$\Delta\xi$ (km s^{-1})	–0.37	–0.49
Δ[Fe/H]	0.09	0.28
Δ[O/Fe] (6300)	0.06	0.23
Δ[O/Fe] (7774)	–0.28	–0.86
Δ[Na/Fe]	–0.02	–0.02
Δ[Mg/Fe]	–0.08	–0.12
Δ[Al/Fe]	–0.06	–0.08
Δ[Si/Fe]	–0.06	–0.13
Δ[Ca/Fe]	–0.05	0.04
Δ[Sc/Fe]	0.04	0.16
Δ[Ti/Fe]	0.01	0.02
Δ[Cr/Fe]	–0.01	0.05
Δ[Co/Fe]	0.02	0.04
Δ[Ni/Fe]	0.01	0.04
Δ[Ba/Fe]	0.15	0.33
Δ[α/Fe]	0.04	0.05

with

$$\log \mathcal{F}_{50} = 8.264 - 3.076\,(V-R)_0 \;\; \text{for} \;\; (V-R)_0 < 1.3 \qquad (2)$$

This calibration relation is appropriate for the range of colours spanned by our program stars (see Table 2). The absolute chromospheric line fluxes were subsequently corrected for incipient photospheric contribution:

$$\mathcal{F}'_{\rm K/H} = \mathcal{F}_{\rm K/H} - \mathcal{F}^{\rm RE}_{\rm K/H} \qquad (3)$$

The K and H indices, $\mathcal{F}^{\rm RE}_{\rm K/H}$, are taken from the radiative equilibrium model atmospheres computed for 3 GK giant stars by Kelch et al. (1978). The "activity index", $R_{\rm HK}$, defined as the radiative loss in the Ca II H+K lines in units of the bolometric luminosity is given by:

$$R_{\rm HK} = \frac{\mathcal{F}'_{\rm K} + \mathcal{F}'_{\rm H}}{\sigma T^4_{\rm eff}} \qquad (4)$$

We use the excitation temperature as an estimate of $T_{\rm eff}$ in equation (4), but note that adopting the colour temperatures given by the $(B-V)$ index would not significantly affect our results.

In addition, we define as a "secondary" indicator of stellar activity, $R_{\rm X}$, given as the ratio between the X-ray and the bolometric luminosities. The latter quantity was derived from evolutionary tracks (Sect. 5.5), while the X-ray data are taken from the *ROSAT* all-sky survey (Dempsey et al. 1993, 1997). These "quiescent" X-ray luminosities in the 0.1–2.4 keV energy range have been rescaled to our more accurate *Hipparcos* distances (Table 10). The major drawback of this activity indicator is that it may not be representative of the stellar activity level at the epoch of the spectroscopic observations, a fact which might contribute to the scatter seen in the plot of $R_{\rm HK}$ against $R_{\rm X}$ (Fig. 5). Note that $R_{\rm X}$ is always well below the empirical threshold defining the "saturation limit" for the X-ray emission in RS CVn binaries ($\sim 10^{-3}$; Dempsey et al. 1993). The measurements of the activity indices are summarized in Table 7. Finally, we define as an indicator of stellar spottedness the maximum amplitude of the wave-like photometric variations in V band, $\Delta V_{\rm wave}$ (values from Strassmeier et al. 1993). Figure 5 suggests that the incidence of these photospheric features scales (possibly in a non-linear way) with the stellar activity level. Figure 6 shows the abundance ratios determined from Method 1 as a function of $R_{\rm HK}$. As found for the other activity indicators, there is no statistically significant correlation between the abundance ratios and the stellar activity level.

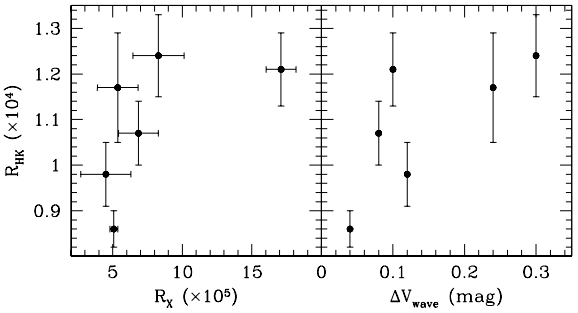

Fig. 5. Dependence of $R_{\rm HK}$ on $R_{\rm X}$ (*left-hand panel*) and on the maximum amplitude of the wave-like photometric variations in V band (*right-hand panel*).

5.2. Discrepancies in the temperature determinations: activity or binarity?

The excitation temperatures are found to be systematically *higher* than the values derived from photometric data (Table 2). This disagreement is more severe for temperatures determined from $(V-R)$ and $(V-I)$ ($\overline{\Delta T} \approx 175$ K) than from $(B-V)$ ($\overline{\Delta T} \approx 65$ K).[4]

[4] Note that interstellar extinction is not a major issue here; an uncertainty of 30% in $A(V)$ would typically translate into an error of 30 K in the colour temperatures.

Chromospheric activity is likely to affect the emergent photospheric spectral energy distribution and thus it might induce this discrepancy. To test this hypothesis, we show in Fig. 7 the difference between the excitation and colour temperatures, as a function of $R_{\rm HK}$, $R_{\rm X}$, and $\Delta V_{\rm wave}$. There is a suggestive indication, in particular from the Ca II H+K data, that the temperature discrepancy increases with the stellar activity level. This result is in line with the recognition that chromospherically active stars exhibit $(V-R)$ and $(V-I)$ colour excesses of about 0.06–0.10 mag compared to otherwise similar, but inactive stars (Fekel, Moffett, & Henry 1986). On the contrary, the much lower temperature discrepancy suggested for the $(B-V)$ index might be accounted for by differences in the $(B-V)$ vs. $T_{\rm eff}$ calibration chosen (Alonso et al. 1999).

The most straightforward explanation for these colour excesses are photospheric spots, which are ubiquitous in RS CVn binaries and cover a substantial fraction of the stellar surface (up to 60%: O'Neal, Saar, & Neff 1996). We examined this possibility by creating a composite, synthetic Kurucz spectrum which is the sum of two normalized components with $T_{\rm eff}$ = 3830 and 4830 K for the spot and photosphere, respectively. We can reasonably assume that the flux emerging from the spots is adequately described by a Kurucz model (see, e.g., Solanki & Unruh 1998 in the case of sunspots). We follow the method of Neff, O'Neal, & Saar (1995) and consider a single spot lying in the center of the stellar disk (i.e., no limb-darkening was included) and with a covering factor, f_s = 30 or 50%. We then performed on this composite spectrum the same analysis as for the active binaries. We also computed the expected colour excesses (and resulting temperatures) from the Kurucz models after convolution with the appropriate filter functions. Table 8 gives the colour and temperature differences compared to the values that would result for a spotless photosphere. Spots have a roughly similar quantitative effect on the temperatures derived from spectroscopic and photometric data, and are unable to explain the distinct behaviour of $(B-V)$ and $(V-R)$ at high activity levels seen in Fig. 7. Although a more detailed treatment is warranted, an interpretation of the temperature discrepancies in terms of spots is therefore not supported by our calculations (see also Fekel et al. 1986). The temperature discrepancies are likely to be a manifestation of activity processes, but the lack of correlation between the temperature differences

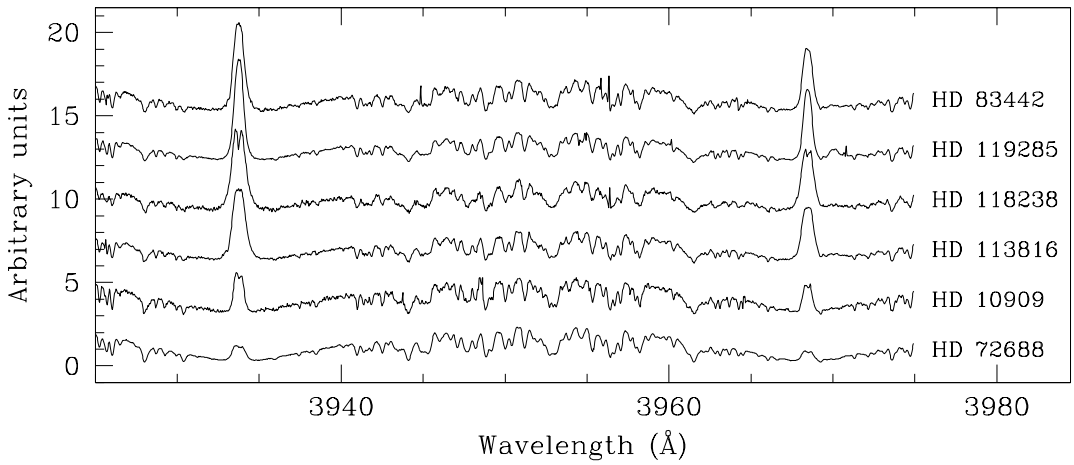

Fig. 4. Ca II H+K profiles for our program stars, ordered as a function of decreasing $R_{\rm HK}$ (*from top to bottom*; see Table 7). The spectra have been normalized to f_{50} (see text) and vertically shifted by a constant value for the sake of clarity.

Table 7. Activity indices.

Name	$(V–R)_0$ (mag)	$T_{\rm eff}$[a] (K)	$\log \mathcal{F}_{\rm K}$	$\log \mathcal{F}_{\rm H}$	$\log \mathcal{F}'_{\rm K}$	$\log \mathcal{F}'_{\rm H}$	$R_{\rm HK}$[b]	$R_{\rm X}$
			(erg cm^{-2} s^{-1})		(erg cm^{-2} s^{-1})		($\times 10^4$)	($\times 10^5$)
HD 10909 (UV For)	0.755	4830±87	6.264	6.104	6.252	6.090	0.98±0.07	4.51±1.80
HD 72688 (VX Pyx)	0.692	5045±62	6.297	6.116	6.281	6.095	0.86±0.04	5.08±0.28
HD 83442 (IN Vel)	0.862	4715±87	6.331	6.139	6.326	6.133	1.24±0.09	8.29±1.84
HD 113816 (IS Vir)	0.887	4700±77	6.254	6.077	6.249	6.071	1.07±0.07	6.85±1.44
HD 118238 (V764 Cen)	0.911	4575±119	6.247	6.068	6.242	6.062	1.17±0.12	5.36±1.46
HD 119285 (V851 Cen)	0.860	4770±77	6.337	6.149	6.332	6.143	1.21±0.08	17.1±1.07

[a] Values obtained with Method 1.
[b] The uncertainties were obtained after propagation of the errors on the absolute emission-line fluxes and effective temperatures.

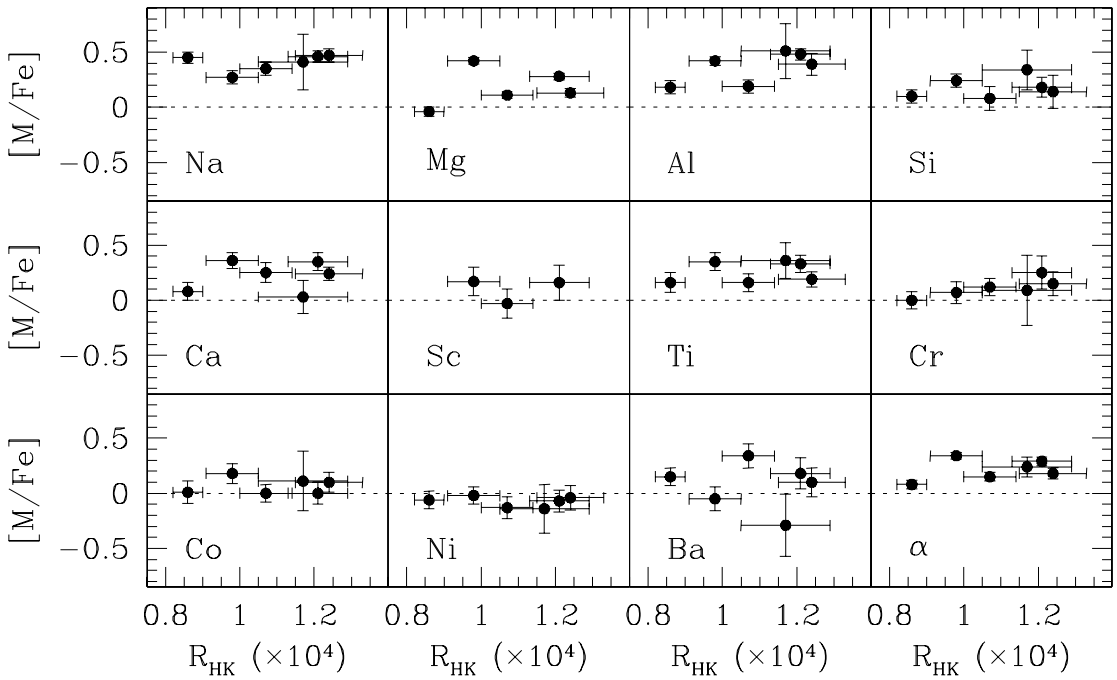

Fig. 6. Abundances (derived from Method 1) as a function of the activity index $R_{\rm HK}$.

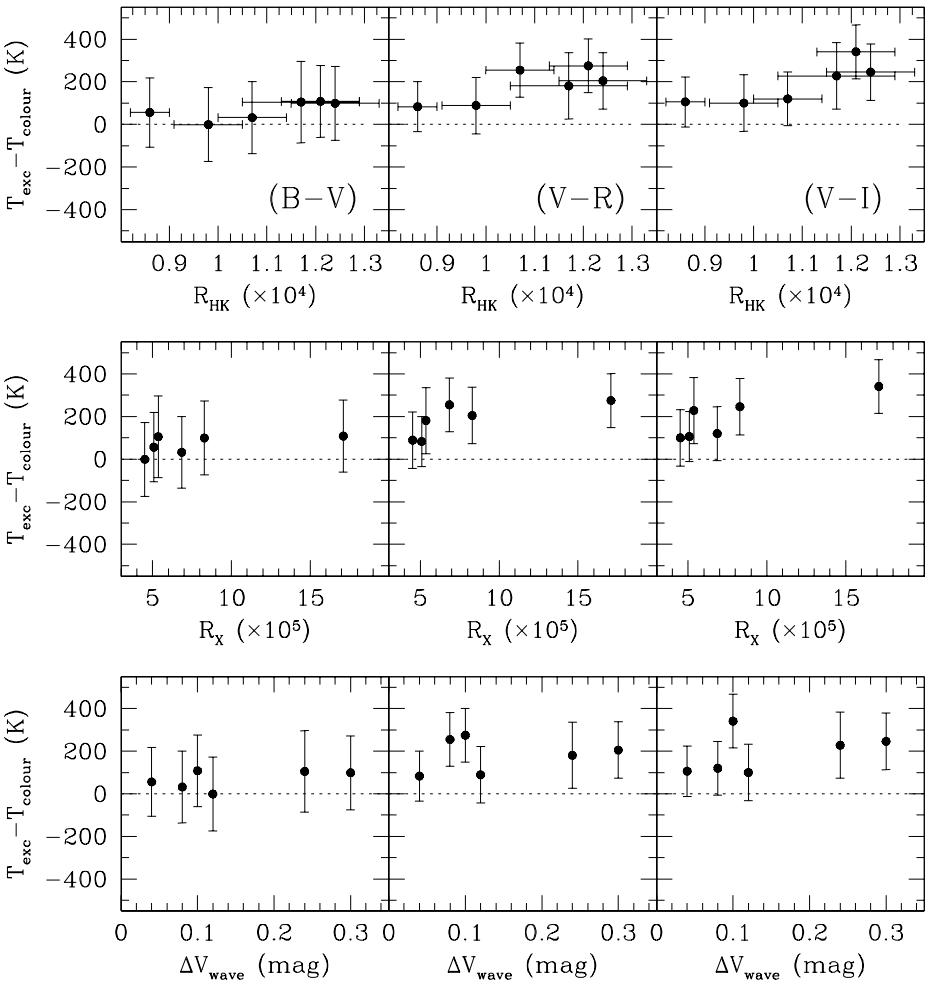

Fig. 7. Differences between the excitation and colour temperatures, as a function of the activity indices $R_{\rm HK}$ (*top panels*), $R_{\rm X}$ (*middle panels*), and maximum amplitude of the wave-like photometric variations in V band, $\Delta V_{\rm wave}$ (*bottom panels*). The variations are shown for temperatures derived from $(B-V)$ (*left-hand panels*), $(V-R)$ (*middle panels*), and $(V-I)$ data (*right-hand panels*).

Table 8. Effect of cool spots on the mean colours, as well as on the excitation and colour temperatures.

f_s	$\Delta(B-V)_0$ (mag)	$\Delta(V-R)_0$ (mag)	$\Delta(V-I)_0$ (mag)	$\Delta T_{\rm exc}$ (K)	$\Delta T(B-V)$ (K)	$\Delta T(V-R)$ (K)	$\Delta T(V-I)$ (K)
0.3	0.026	0.022	0.065	100	51	60	113
0.5	0.056	0.046	0.132	200	109	123	221

and $\Delta V_{\rm wave}$ also suggests that they may not be strictly related to spots *per se*.

A cooler secondary component significantly contributing to the overall spectral energy distribution would lead to spuriously low colour temperatures.[5] There are indeed indications for such low-mass companions for some stars among our sample: HD 113816 (K5 V; Fekel et al. 2002) and HD 119285 (M3 V; Saar, Nordström, & Andersen 1990). The sensitivity of the photometric colours on the nature of the secondary has been already quantitatively addressed in Paper I. It was found that such effects could be substantial for dwarfs, but would typically

[5] An enlightening, albeit extreme, illustration is provided by HD 101379 (K3 III, GT Mus). This system comprises a pair of eclipsing A dwarfs (Murdoch et al. 1995) and was initially included in our study. It is classified as single lined by Strassmeier et al. (1993). From the 3 photometric indices, we obtain colour temperatures in the range 5210–5270 K. These values are about 650 K higher than the excitation temperature, and are clearly inconsistent with the spectral type. Conversely, results obtained with Method 1 suggest an iron content ([Fe/H] ≈ -0.45) difficult to reconcile with the young stellar age derived from theoretical isochrones. This low metallicity is likely to be spurious, and to result from a dilution of the continuum by the hot, early-type eclipsing binary (which is only 0.8 mag fainter in V).

lead to differences below 70 K for giants. Regardless of the seemingly important role played by activity discussed above, binarity can therefore hardly account for the large differences observed in our subgiant stars (up to 340 K).

5.3. Lithium abundance

The lithium abundance was determined from a spectral synthesis of the Li I λ6708 doublet. This more sophisticated approach was made necessary by the blended nature of this doublet at our instrumental resolution and by its complex atomic structure. The synthetic spectra were generated using the MOOG software and the line list of Cunha, Smith, & Lambert (1995), while the atmospheric parameters used were those determined previously (Table 3). Because of the weakness in the solar spectrum of the spectral features of interest, a relative calibration of the gf-values as was done for the other spectral lines was not attempted. Instead, we use for lithium the laboratory atomic data quoted in Smith, Lambert, & Nissen (1998). As discussed by these authors, the gf-values are thought to be exceptionally accurate (the ^{6}Li isotope was not considered). For the CN molecules and other atomic lines in the spectral domain of interest, we adopt the oscillator strengths of Cunha et al. (1995). The projected rotational velocity, $v \sin i$, along with the iron and lithium abundances, were adjusted until a satisfactory Gaussian fit of the blend primarily formed by Fe I λ6707.4 and the Li doublet was achieved (see Fig. 8). The fit quality is largely insensitive to the abundance of the other chemical species, and solar values were assumed. A very small velocity shift ($\lesssim$1 km s^{-1}) was applied to account for an imperfect correction of the stellar radial velocity. Mean macroturbulent velocities, ζ, appropriate to the stellar spectral type and luminosity class were used (Fekel 1997). Instrumental broadening was also taken into account. A close agreement was found in all cases betweeen the iron abundance given by the weak Fe I λ6707.4 line and the mean values in Table 3. Likewise, the $v \sin i$ values used are in good agreement with previous estimates in the literature (Table 1). NLTE corrections interpolated from the grids of Carlsson et al. (1994) for the relevant atmospheric parameters (typically $\Delta\epsilon = +0.2$ dex) were applied to the lithium abundances (see Table 9). Owing to the weakness of the Li I λ6708 feature in HD 10909 and HD 83442, only upper limits could be determined. Differences between our abundances (prior to NLTE corrections) and previous estimates in the literature (Barrado y Navascués et al. 1998; Costa et al. 2002; Fekel & Balachandran 1993; Randich et al. 1993, 1994; Soderblom 1985: Strassmeier et al. 2000) can generally be accounted for by differences in the temperature scale.

Several stars among our sample exhibit a lithium abundance not only higher than what would be expected for such evolved objects, but also higher than single stars with similar characteristics (do Nascimento et al. 2000). Echoing previous investigations, our data do not show any dependence of the Li content on the stellar evolutionary status, mass or activity (e.g., Randich et al. 1993, 1994). The Li abundance is sensitive to a variety of competing physical processes, however, and we feel that meaningful conclusions can only be drawn by seeking

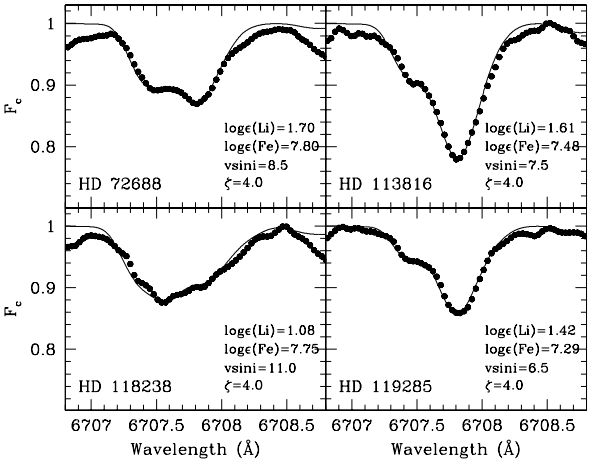

Fig. 8. Spectral synthesis of the Li I λ6708 doublet. The atmospheric parameters derived from Method 1 have been used. The resulting lithium and iron abundances (the latter given by Fe I λ6707.4), $v \sin i$, and macroturbulent velocity (ζ) are indicated (velocities in km s^{-1}).

Table 9. NLTE lithium abundances. We use the usual notation: $\log \epsilon(\mathrm{Li}) = \log \mathcal{N}(\mathrm{Li}) - 12.0$. The uncertainties were determined as detailed in Sect. 4.

Name	log ϵ(Li)	
	Method 1	Method 2
HD 10909 (UV For)	$\lesssim$ 0.6	$\lesssim$ 0.6
HD 72688 (VX Pyx)	1.70±0.12	1.66±0.19
HD 83442 (IN Vel)	$\lesssim$ 0.6	$\lesssim$ 0.6
HD 113816 (IS Vir)	1.61±0.15	1.58±0.21
HD 118238 (V764 Cen)	1.08±0.20	0.92±0.33
HD 119285 (V851 Cen)	1.42±0.14	1.30±0.21

statistical trends in much larger samples than analyzed here. We simply note a tentative indication that systems with higher rotational velocities might have retained more of their primordial Li (Fig. 9; see also Barrado y Navascués et al. 1998). We do not find evidence for systems with synchronized orbits to be less lithium depleted, as would be expected if internal mixing was inhibited in tidally locked binaries (Zahn 1994). This mechanism is perhaps more likely to explain the lack of very lithium-poor stars in close binary systems (Costa et al. 2002).

5.4. Stellar Kinematics

The space components (U, V, W) were computed from *Hipparcos* data following Johnson & Soderblom (1987). They were subsequently corrected for the effect of differential galactic rotation (Scheffler & Elsässer 1988), by adopting a solar galactocentric distance of 8.5 kpc and a circular velocity of 220 km s^{-1}. All kinematic data are quoted in Table 10 and refer to the LSR at the star's position and to a right-handed reference system (i.e., with $\boldsymbol{U}$ oriented towards the galactic centre). Rough estimates of the kinematic ages are also given. A solar motion $(U, V, W)_\odot = (10.0, 5.2, 7.2)$ km s^{-1} was assumed

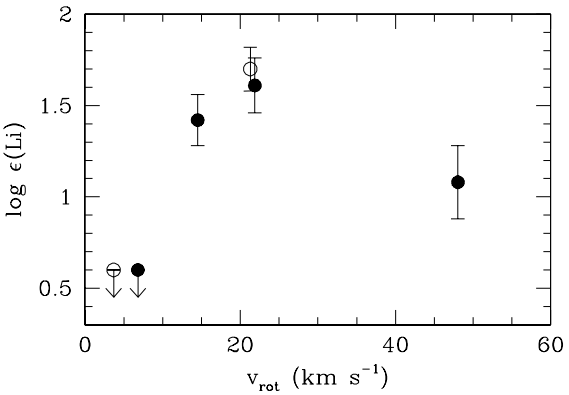

Fig. 9. Lithium abundance as a function of the rotational velocity. The latter quantity was calculated using our effective temperatures (Method 1), the luminosities given by evolutionary tracks (Sect.5.5), and the rotational periods (Table 1). The synchronous and asynchronous systems are plotted as filled and open circles, respectively.

(Dehnen & Binney 1998). The peculiar space velocity, S, is given by: $S = (U^2 + V^2 + W^2)^{1/2}$, and is shown as a function of [Fe/H] in Fig. 10. The kinematic properties of HD 72688, HD 113816, and HD 118238 suggest that they belong to the thin disk population. The situation is less clear for HD 10909, HD 83442, and HD 119285 which display at least one velocity component typical of the thick disk or halo (e.g., Soubiran 1993).[6]

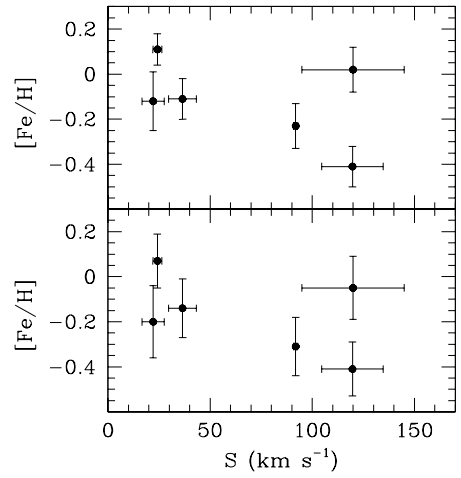

Fig. 10. [Fe/H] as a function of the peculiar space velocities for Method 1 (*top*) and Method 2 (*bottom*).

5.5. Evolutionary status

A comparison with theoretical isochrones allows us to examine the stellar evolutionary status and provides a consistency test on our derived surface gravities. In virtue of the departures exhibited by most stars in our sample from a scaled-solar chemical composition (Fig. 1), we use the recent set of isochrones for α-element enhanced mixtures of Kim et al. (2002). These isochrones have been constructed for an α-element abundance ([α/Fe] = +0.3) that is a better match to the overabundances observed than the value [α/Fe] = +0.5 used by Salasnich et al. (2000). For HD 72688, we use the isochrones for scaled-solar mixture of Yi et al. (2001). Both set of evolutionary models use the same input physics, up-to-date opacities and equations of state, and are evolved from the pre-main-sequence birthline to the onset of helium burning in the core.

The positions of the stars in the HR diagrams for the appropriate Fe and [α/Fe] abundances are shown in Fig. 11. The metallicity of the isochrone was chosen to match as closely as possible our spectroscopic values (allowance was made for the different solar iron abundances assumed). The absolute magnitudes are not significantly affected by the presence of a faint, main-sequence companion. Our stars share a very similar evolutionary status and are all starting to ascend the red giant branch. Estimates of the stellar masses were derived from the evolutionary tracks (Table 10), and suggest that these stars have evolved from main-sequence progenitors with masses ranging from about 1.0 to 3.3 $M_\odot$ (i.e., of spectral type G2–A0). The evolutionary age derived from Method 2 for HD 119285 appears uncomfortably large and points to an underestimated effective temperature. However, the loci in the M_V-$T_{\rm eff}$ plane are very sensitive to the somewhat subjective choice of the isochrone metallicity. Furthermore, if HD 119285 belongs to the thick disk (a possibility that cannot be ruled out from its kinematics; Table 10), then we would expect it to be about 12 Gyr old. This value is, within the uncertainties, consistent with the isochrones. The evolutionary ages are in fair agreement with the kinematic ages (Table 10), and are shown as a function of [Fe/H] in Fig. 12.

A comparison between the gravities derived from the ionization equilibrium of the Fe lines and from the evolutionary tracks is shown in Fig. 13. A reasonable agreement is found, although there is a clear indication that the spectroscopic gravities are systematically lower by about 0.15 dex. Whatever the cause of this putative discrepancy (see Allende Pietro et al. 1999 for a thorough discussion), we simply stress here that such a gravity offset would have little impact on the abundance patterns (Δ[M/Fe] $\lesssim$ 0.05 dex) and would thus not affect the conclusions presented in this paper.

6. Conclusions

The temperatures derived from $(V-R)$ and $(V-I)$ colour indices appear to be affected in our sample by activity processes whose exact nature remains to be identified. On the contrary, a fair agreement between the excitation temperatures and the values derived from the $(B-V)$ data is found, suggesting that this colour index might be a more robust indicator of the effective temperature in chromospherically active binaries (provided that the metallicity is known with reasonable accuracy).

Irrespective of the method used, our study suggests that active binaries may not be as iron-deficient as previously thought (see also Ottmann et al. 1998). The physical mechanisms lead-

[6] see also: http://physique.obs-besancon.fr/modele/description.html

Table 10. Kinematic data, along with kinematic ($\tau_{\rm kin}$; Scheffler & Elsässer 1988) and evolutionary ages ($\tau_{\rm iso}$). No determination of $\tau_{\rm iso}$ from Method 2 was possible for HD 119285 (see Fig. 11). The last row gives the stellar mass derived from the evolutionary tracks (Method 1).

	HD 10909	HD 72688	HD 83442	HD 113816	HD 118238	HD 119285
α (1950.0) (°)	26.09	127.75	143.81	195.96	203.32	205.14
δ (1950.0) (°)	–24.26	–34.46	–41.80	–4.58	–33.22	–61.12
l (°)	201.96	254.82	268.75	309.96	313.53	309.19
b (°)	–77.16	3.14	7.61	57.82	28.47	0.86
π (mas)	7.67±1.10	7.65±0.59	3.50±1.19	3.33±1.01	1.97±1.19	13.13±1.34
$\mu_\alpha \cos\delta$ (mas)	151.03±1.01	–18.26±0.43	–72.49±0.83	–3.19±1.03	–1.98±1.03	22.07±1.01
μ_δ (mas)	97.42±0.69	3.27±0.47	19.53±0.94	–19.23±0.71	–4.43±0.80	16.68±1.03
v_r (km s^{-1})[a]	–4.62±1.65	6.40±4.95	48.7±3.0	19.0±4.0	9.3±3.0	93.27±0.65
U (km s^{-1})	–116.7±15.5	–16.6±1.5	–94.4±30.9	8.5±3.3	2.6±2.9	57.4±0.9
V (km s^{-1})	–15.9±1.8	–9.6±4.8	–57.5±3.4	–35.1±7.0	–18.9±5.5	–71.8±1.0
W (km s^{-1})	21.1±3.8	–14.7±0.8	–46.5±15.6	–5.3±5.5	–11.1±5.5	–1.4±0.7
S (km s^{-1})	119.7±15.1	24.2±2.2	120.0±25.1	36.5±6.8	22.1±5.5	91.9±1.0
$\tau_{\rm kin}$ (Gyr)	$\gtrsim 9$	$\sim$0.3	$\gtrsim 9$	$\sim$1	$\sim$0.2	$\sim$9
$\tau_{\rm iso}$ (Method 1) (Gyr)	7^{+6}_{-3}	$0.6^{+0.1}_{-0.1}$	$2.5^{+3.0}_{-1.5}$	$1.0^{+1.5}_{-0.5}$	$0.3^{+1.2}_{-0.2}$	15^{+5}_{-5}
$\tau_{\rm iso}$ (Method 2) (Gyr)	7^{+8}_{-4}	$0.6^{+0.2}_{-0.2}$	$4.0^{+6.0}_{-2.5}$	$1.2^{+1.4}_{-0.6}$	$0.4^{+2.6}_{-0.3}$	
M ($M_\odot$)	1.2	2.6	1.6	2.1	3.3:	1.0

[a] Radial velocities of the center of mass from Strassmeier et al. (1993) and references therein, except for HD 10909 and HD 72688 (de Meideros & Mayor 1999).

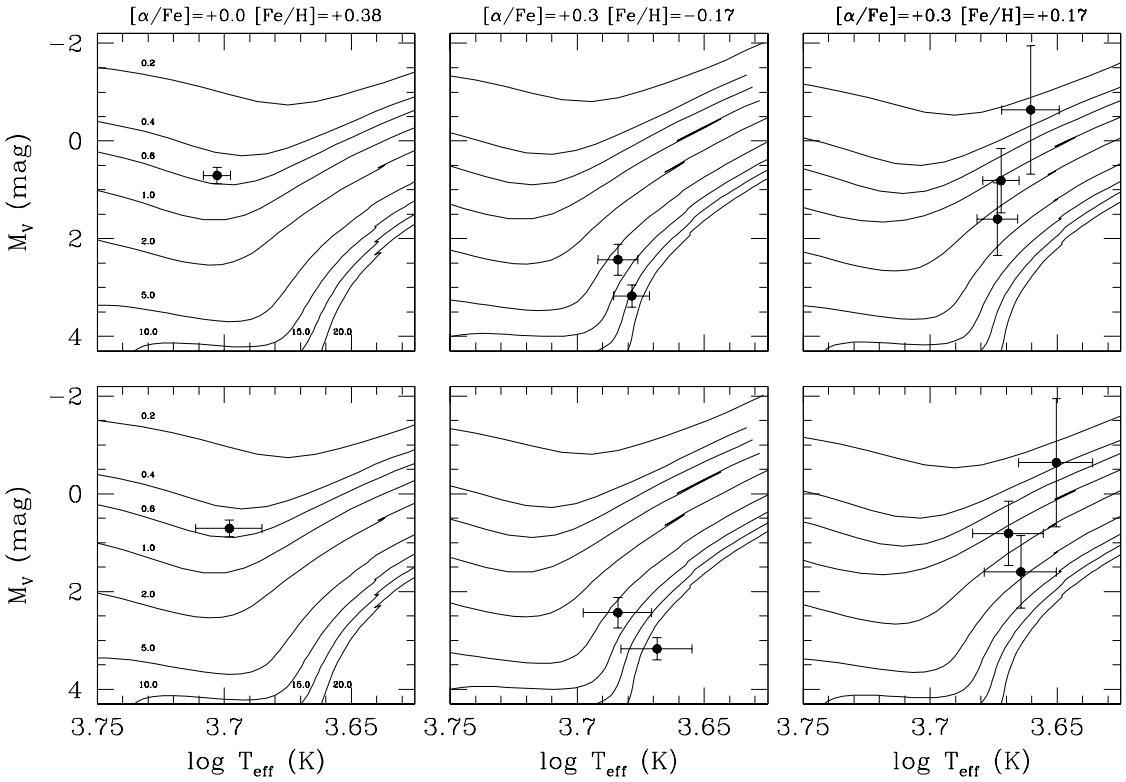

Fig. 11. Positions of the program stars in the HR diagrams for Method 1 (*top*) and Method 2 (*bottom*). The theoretical isochrones are shown for [α/Fe]=0.0 and [Fe/H]=+0.38 (*left-hand panels*; HD 72688), [α/Fe]=+0.3 and [Fe/H]=−0.17 (*middle panels*; from top to bottom: HD 10909 and HD 119285), as well as [α/Fe]=+0.3 and [Fe/H]=+0.17 (*right-hand panels*; from top to bottom: HD 118238, HD 113816, and HD 83442). The metallicity of the isochrones refers to a solar iron abundance: $\log \epsilon_\odot$(Fe)=7.50 (Yi et al. 2001; Kim et al. 2002). The age of the isochrones (in Gyr) is indicated in the left-hand panels.

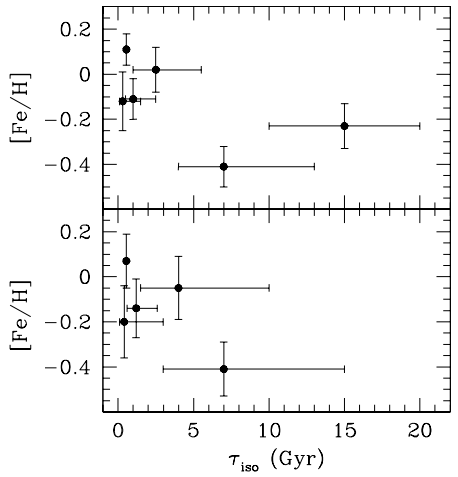

Fig. 12. [Fe/H] as a function of the ages derived from the theoretical isochrones for Method 1 (*top*) and Method 2 (*bottom*). For HD 119285, no age estimate from the evolutionary tracks was possible from Method 2 (see Fig. 11).

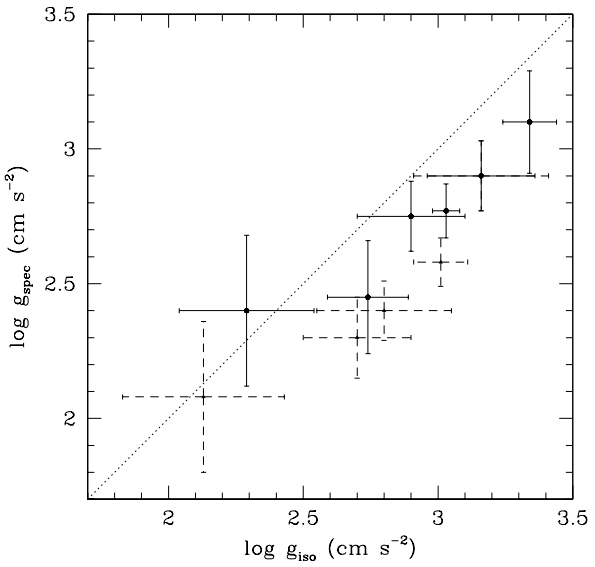

Fig. 13. Comparison between the gravities given by the theoretical isochrones and the values derived from Method 1 (*solid*) and Method 2 (*dashed*). In the latter case, no estimate of the gravity from the evolutionary tracks was possible for HD 119285 (see Fig. 11). The error bars for the theoretical gravities were derived from the uncertainties on the position of the stars in the HR diagrams.

ing to the noticeable metal enrichment observed remain to be identified, although an interpretation in terms of nucleosynthesis yields remains viable. In particular, the gradient between [α/Fe] and [Fe/H] is much steeper than for thin disk dwarfs (e.g., Reddy et al. 2003), but is reminiscent of the thick disk population (e.g., Feltzing, Bensby, & Lundström 2003). Part of the gradient could therefore be due in our sample to a mix of the 2 populations (thin and thick disk stars; Sect. 5.4). On the other hand, these stars are presumably not evolved enough to have experienced deep convective mixing (as supported by the high Li abundance in some of them; Table 9). The abundance peculiarities observed are thus hard to explain in the framework of standard evolutionary theory.

Our data do not show a clear correlation between the abundance ratios and the activity level (Fig. 6), therefore firm conclusions regarding the potential role played by chromospheric activity in inducing the overabundances observed must await the analysis of a much larger sample. Our exploratory calculations suggest that chromospheric heating of the upper photosphere is unlikely to significantly affect the abundance patterns. A more sophisticated and rigorous approach (e.g., relaxing the assumption of LTE) is, however, needed to investigate this issue further and to establish the importance of other physical processes causally related to activity.

Acknowledgements. This research was supported through a European Community Marie Curie Fellowship. G. M. and I. P. acknowledge financial support from ASI (Italian Space Agency) and MIUR (Ministero della Istruzione, dell'Università e della Ricerca). We made use of the Simbad database operated at CDS, Strasbourg, France. We wish to thank an anonymous referee for useful comments.

Appendix A: Line list and oscillator strengths

Table A.1 gives for each spectral line the wavelength, excitation potential (Kurucz & Bell 1995), the adopted $\log gf$-value (see Sect. 3), and the EW measurements. Kurucz solar abundances are listed along with the element symbols. Fig. A.1 presents a comparison between our gf-values and previous determinations in the literature after rescaling to Kurucz solar abundances (Edvardsson et al. 1993; Feltzing & Gonzalez 2001; Kurucz & Bell 1995; Neuforge-Verheecke & Magain 1997; Reddy et al. 2003). Except for Kurucz & Bell (1995), all gf-values have also been calibrated on the Sun. Neuforge-Verheecke & Magain (1997) values were determined from the Liège Solar Atlas and by using the solar model of Holweger & Müller (1974). Feltzing & Gonzalez (2001) derived their values from the Kitt Peak Solar Flux Atlas (Kurucz, Furenlid, & Brault 1984) and a MARCS solar model (Gustafsson et al. 1975). Edvardsson et al. (1993) and Reddy et al. (2003) used a purpose-built solar model and an ATLAS9 Kurucz model, respectively. They both used a solar spectrum obtained as part of their observational programs. In contrast, the gf-values of Kurucz & Bell (1995) come from a variety of experimental studies, and are therefore highly heterogeneous. This is likely to be reflected in the large scatter seen in Fig. A.1 (*bottom*).

The agreement between our values and those found in the literature using a similar approach is reasonably good (the differences never exceed 0.25 dex). The agreement is in particular excellent with Neuforge-Verheecke & Magain (1997) and Reddy et al. (2003). However, a systematic offset for elements heavier than Ca is found with Edvardsson et al. (1993) and Feltzing & Gonzalez (2001). There is some indication for an increasing offset between Edvardsson et al. (1993) values and ours for stronger lines. This discrepancy might stem from our neglect of some damping processes in the determination of the solar abundances (e.g., van der Walls broadening implemented without enhancement factors), as also done by

Neuforge-Verheecke & Magain (1997) and Reddy et al. (2003). However, because our analysis of RS CVn binaries is strictly differential with respect to the Sun, where lines have comparable strength, this offset has no bearing on our derived abundances.

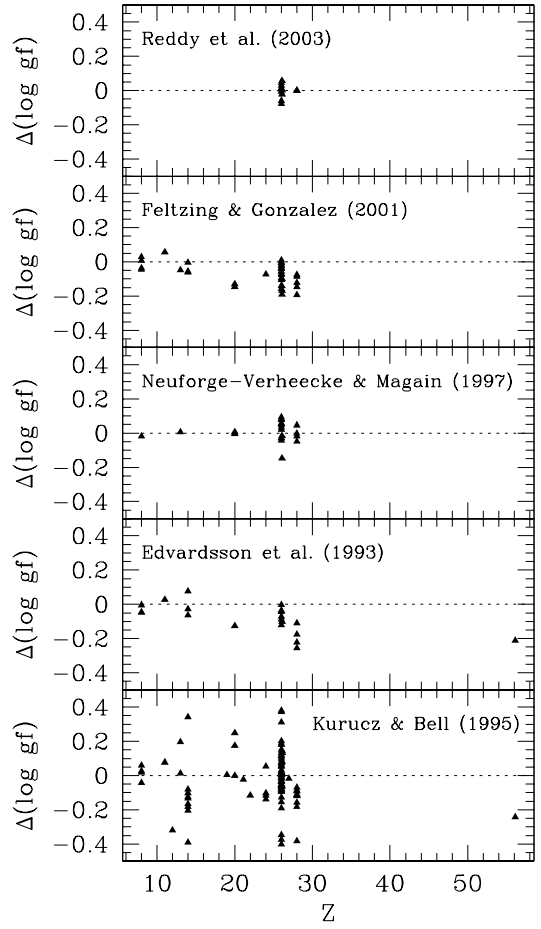

Fig. A.1. Comparison between our calibrated gf-values and previous determinations in the literature. The differences are given in the form $\Delta(\log gf)$ = $\log gf$(literature) – $\log gf$(this study). The values of Kurucz & Bell (1995) for Fe I λ7780 and Si I λ6029 are off-scale, and are likely erroneous.

References

Allende Prieto, C., García López, R., Lambert, D. L., & Gustafsson, B. 1999, ApJ, 527, 879

Allende Prieto, C., Lambert, D. L., & Asplund, M. 2001, ApJ, 556, L63

Alonso, A., Arribas, S., & Martínez-Roger, C. 1999, A&AS, 140, 261

Alonso, A., Arribas, S., & Martínez-Roger, C. 2001, A&A, 376, 1039

Arenou, F., Grenon, M., & Gómez, A. 1992, A&A, 258, 104

Audard, M., Güdel, M., Sres, A., Raassen, A. J. J., & Mewe, R. 2003, A&A, 398, 1137

Barklem, P. S., Stempels, H. C., Allende Prieto, C., et al. 2002, A&A, 385, 951

Barrado y Navascués, D., de Castro, E., Fernández-Figueroa, M. J., Cornide, M., & García López, R. J. 1998, A&A, 337, 739

Bessell, M. S. 1979, PASP, 91, 589

Cardelli, J. A., Clayton, G. C., & Mathis, J. S. 1989, ApJ, 345, 245

Carlsson, M., Rutten, R. J., Bruls, J. H. M. J., & Shchukina, N. G. 1994, A&A, 288, 860

Cavallo, R. M., Pilachowski, C. A., & Rebolo, R. 1997, PASP, 109, 226

Costa, J. M., da Silva, L., do Nascimento Jr., J. D., & de Medeiros, J. R. 2002, A&A, 382, 1016

Cox, A. N., (ed.) 2000, Allen's astrophysical quantities, 4th ed, (Springer-Verlag: New York)

Cunha, K., Smith, V. V., & Lambert, D. L. 1995, ApJ, 452, 634

Cutispoto, G., Messina, S., & Rodonò, M. 2001, A&A, 367, 910

Dehnen, W., & Binney, J. J. 1998, MNRAS 298, 387

de Medeiros, J. R., & Mayor, M. 1999, A&AS, 139, 433

Dempsey, R. C., Linsky, J. L., Fleming, T. A., & Schmitt, J. H. M. M. 1993, ApJS, 86, 599

Dempsey, R. C., Linsky, J. L., Fleming, T. A., & Schmitt, J. H. M. M. 1997, ApJ, 478, 358

do Nascimento Jr., J. D., Charbonnel, C., Lèbre, A., de Laverny, P., & de Medeiros, J. R. 2000, A&A, 357, 931

Donati, J.-F., Henry, G. W., & Hall, D. S. 1995, A&A, 293, 107

Drake, J. J. 1991, MNRAS, 251, 369

Edvardsson, B., Andersen, J., Gustafsson, B., et al. 1993, A&A, 275, 101

Favata, F., Micela, G., Sciortino, S., & Morale, F. 1997, A&A, 324, 998

Favata, F., & Micela, G. 2003, Space Science Reviews, in press (astro-ph/0302565)

Fekel, F. C., Moffett, T. J., & Henry, G. W. 1986, ApJS, 60, 551

Fekel, F. C., & Balachandran, S. 1993, ApJ, 403, 708

Fekel, F. C. 1997, PASP, 109, 514

Fekel, F. C., Henry, G. W., Brooks, K., & Hall, D. S. 2001, AJ, 122, 991

Fekel, F. C., Henry, G. W., Eaton, J. A., Sperauskas, J., & Hall, D. S. 2002, AJ, 124, 1064

Feltzing, S., & Gonzalez, G. 2001, A&A, 367, 253

Feltzing, S., Bensby, T., & Lundström, I. 2003, A&A, 397, L1

Fuhrmann, K., Axer, M., & Gehren, T. 1993, A&A, 271, 451

Fulbright, J. P., & Johnson, J. A. 2003, ApJ, in press (astro-ph/0307063)

Gehren, T., Ottmann, R., & Reetz, J. 1999, A&A, 344, 221

Giménez, A., Reglero, V., de Castro, E., & Fernández-Figueroa, M. J. 1991, A&A, 248, 563

Gratton, R. G., & Sneden, C. 1987, A&A, 178, 179

Gratton, R. G., Carretta, E., Eriksson, K., & Gustafsson, B. 1999, A&A, 350, 955

Grevesse, N., & Sauval, A. J. 1998, Space Science Rev., 85, 161

Gustafsson, B., Bell, R. A., Eriksson, K., & Nordlund, Å. 1975, A&A, 42, 407

Hinkle, K., Wallace, L., Valenti, J., & Harmer, D. 2000, Visible and Near Infrared Atlas of the Arcturus Spectrum 3727-9300 Å, (San Francisco: ASP)

Holweger, H., & Müller, E. A. 1974, Solar Physics, 39, 19

Johnson, D. R. H., & Soderblom, D. R. 1987, AJ, 93, 864

Katz, D., Favata, F., Aigrain, S., & Micela, G. 2003, A&A, 397, 747 (Paper I)

Kelch, W. L., Linsky, J. L., Basri, G. S., et al. 1978, ApJ, 220, 962

Kim, Y.-C., Demarque, P., Yi, S. K., & Alexander, D. R. 2002, ApJS, 143, 499

Kjærgaard, P., Gustafsson, B., Walker, G. A. H., & Hultqvist, L. 1982, A&A, 115, 145

Kupka, F., Piskunov, N., Ryabchikova, T. A., Stempels, H. C., & Weiss, W. W. 1999, A&AS, 138, 119

Table A.1. Calibrated atomic data and EW measurements

λ (Å)	χ (eV)	log gf	EW (mÅ)[a]					
			UV For	VX Pyx	IN Vel	IS Vir	V764 Cen	V851 Cen
O I; log $\epsilon_\odot$(O)=8.93								
6300.304	0.000	–9.778	20.1			23.4		
7771.944	9.147	0.297	65.3	81.6	84.0	92.3	125.1	93.8
7774.166	9.147	0.114	54.4		75.8		120.7	84.2
7775.388	9.147	–0.064	38.7	58.3				53.9
Na I; log $\epsilon_\odot$(Na)=6.33								
6154.226	2.102	–1.637	62.1	103.4	124.3	100.5	139.8	97.0
Mg I; log $\epsilon_\odot$(Mg)=7.49								
5711.088	4.346	–1.514	138.7	139.6	163.9	151.2		152.5
Al I; log $\epsilon_\odot$(Al)=6.47								
6698.673	3.143	–1.843	51.6	59.9	84.5	62.9	95.5	70.5
7835.309	4.022	–0.663	65.0	83.7	111.0	79.8	144.0	92.4
Si I; log $\epsilon_\odot$(Si)=7.55								
5793.073	4.930	–1.894	49.2	75.6	73.2	61.3	86.4	56.0
5948.541	5.083	–1.098	88.0					
6029.869	5.984	–1.553			38.2		42.2	
6155.134	5.620	–0.742	71.5	105.0	91.3	83.9	106.4	74.6
6721.848	5.863	–1.100	41.3	71.6	67.2	56.3	78.0	45.0
7034.901	5.871	–0.779	51.2		69.4			
7680.266	5.863	–0.609	68.5	100.7	85.6	80.0		75.2
7760.628	6.206	–1.356						
8742.446	5.871	–0.448	79.3		91.7			
8892.720	5.984	–0.705	62.0					
Ca I; log $\epsilon_\odot$(Ca)=6.36								
6166.439	2.521	–1.074	103.3	112.2	145.7	131.4	163.0	124.9
6455.598	2.523	–1.350	93.1	106.7	135.6	123.2	154.5	116.0
6499.650	2.523	–0.839	128.2	134.4	171.9	161.6		158.1
Sc II; log $\epsilon_\odot$(Sc)=3.10								
6320.851	1.500	–1.747	21.9			33.1		24.9
Ti I; log $\epsilon_\odot$(Ti)=4.99								
5766.330	3.294	0.370	32.9	41.5	57.4	46.7	80.3	46.1
Cr I; log $\epsilon_\odot$(Cr)=5.67								
5787.965	3.323	–0.138	66.6	85.6	109.8	100.7	136.8	90.7
6882.475	3.438	–0.238	56.7	75.1		90.9		
6882.996	3.438	–0.305	56.3	75.8				80.8
6925.202	3.450	–0.227	60.5	81.4	108.5	94.7		95.9
Fe I; log $\epsilon_\odot$(Fe)=7.67								
5543.937	4.218	–1.155	74.4	101.1	113.5	104.9	136.2	92.8
5638.262	4.221	–0.882	90.3	118.9	134.9	121.7		108.7
5679.025	4.652	–0.863	68.3	90.7	100.4	92.8	117.9	84.0
5732.275	4.992	–1.473	25.3	45.1	40.2			26.1
5806.717	4.608	–0.984	63.2	91.2	97.9	89.8	118.8	76.7

Kupka, F. G., Ryabchikova, T. A., Piskunov, N. E., Stempels, H. C., & Weiss, W. W. 2000, Baltic Astronomy, 9, 590

Kurucz, R. L., Furenlid, I., & Brault, J. 1984, National Solar Observatory Atlas, Sunspot, New Mexico: National Solar Observatory

Kurucz, R. L. 1993, ATLAS9 Stellar Atmosphere Programs and 2 km/s grid. Kurucz CD-ROM No. 13. Cambridge, Mass.: Smithsonian Astrophysical Observatory, 1993, 13

Kurucz, R. L., & Bell, B. 1995, Atomic Line Data (R. L. Kurucz and B. Bell) Kurucz CD-ROM No. 23. Cambridge, Mass.: Smithsonian Astrophysical Observatory, 1995, 23

Lambert, D. L., & Ries, L. M. 1981, ApJ, 248, 228

Lanzafame, A. C., Busà, I., & Rodonò, M. 2000, A&A, 362, 683

Linsky, J. L., Worden, S. P., McClintock, W., & Robertson, R. M. 1979, ApJS, 41, 47

Mäckle, R., Holweger, H., Griffin, R., & Griffin, R. 1975, A&A, 38, 239

McWilliam, A., Preston, G. W., Sneden, C., & Searle, L. 1995, AJ, 109, 2757

Mashonkina, L., Gehren, T., Travaglio, C., & Borkova, T. 2003, A&A 397, 275

Mihalas, D. 1978, in Stellar Atmospheres (2nd ed., Freeman, San Fransisco), p.116

Morale, F., Micela, G., Favata, F., & Sciortino, S. 1996, A&AS, 119, 403

Murdoch, K. A., Hearnshaw, J. B., Kilmartin, P. M., & Gilmore, A. C. 1995, MNRAS, 276, 836

Table A.1. Continued.

λ (Å)	χ (eV)	log gf	EW (mÅ)[a]					
			UV For	VX Pyx	IN Vel	IS Vir	V764 Cen	V851 Cen
5848.123	4.608	–1.282	51.2	76.6	90.0	79.0	97.4	63.8
5855.091	4.608	–1.681		47.7	56.2	48.4	58.1	38.2
5905.689	4.652	–0.860	68.3	93.2	94.8	94.1	130.8	
5909.970	3.211	–2.731	65.5		102.5		117.4	71.4
5927.786	4.652	–1.243			76.1			60.1
5929.667	4.549	–1.332	47.2	74.7	75.5	74.2	91.4	60.3
5930.173	4.652	–0.347	98.5	126.4	131.8	126.3		
5947.503	4.607	–2.059		32.1	33.3			
6078.491	4.796	–0.414	86.0	115.7	124.7	114.2	148.1	99.1
6078.999	4.652	–1.123	58.1	82.4	94.2	86.4	105.0	76.7
6094.364	4.652	–1.749	25.7	49.4		46.9		35.0
6098.280	4.559	–1.940	24.6			45.1		34.3
6151.617	2.176	–3.486	83.1		126.1	123.2		106.3
6165.361	4.143	–1.645	54.9	80.5	91.7	82.0	112.0	67.7
6187.987	3.944	–1.740	66.1	91.6	102.2	94.5	116.0	79.5
6219.279	2.198	–2.551	134.7	161.3				160.4
6252.554	2.404	–1.867	161.5					
6322.690	2.588	–2.503	110.4	134.8		148.5		
6335.328	2.198	–2.432	143.2	167.8				168.1
6336.823	3.687	–0.896	131.3	161.7		172.1		161.6
6436.411	4.187	–2.538		38.1				23.7
6469.213	4.835	–0.774						79.2
6593.871	2.433	–2.342	126.0		179.4	168.2		145.5
6699.162	4.593	–2.172		32.8		25.7		19.0
6713.771	4.796	–1.606		48.7	50.4	43.4		32.2
6725.353	4.104	–2.370	27.8	48.2	54.4	47.1	56.0	33.5
6726.661	4.607	–1.200	53.1	78.8	83.3	78.2	105.2	64.8
6733.151	4.639	–1.594	34.7	57.4	61.4	56.6		44.1
6745.090	4.580	–2.192				30.5		
6750.150	2.424	–2.727	115.4	142.6	163.2	161.1		132.6
6806.847	2.728	–3.265	61.9	91.5	112.8	100.5	138.3	80.7
6810.257	4.607	–1.129	56.0	88.4	94.9	88.9		72.0
6820.369	4.639	–1.289	46.0	77.5	85.1	74.0	104.7	
6843.648	4.549	–0.934	66.8	98.3	102.6	95.7		76.9
6857.243	4.076	–2.203	30.7	54.5	63.1	57.6		41.6
6862.492	4.559	–1.509	37.9	65.1	69.4	68.3		49.9
7022.953	4.191	–1.184			116.2			98.8
7219.678	4.076	–1.715	59.0		90.0	88.8		71.2
7306.556	4.178	–1.684	53.5		95.3	79.3		
7746.587	5.064	–1.379	19.6			41.7		35.2
7748.274	2.949	–1.748	135.2	178.2	198.7	185.1		166.4

Neff, J. E., O'Neal, D., & Saar, S. H. 1995, ApJ, 452, 879
Neuforge-Verheecke, C., & Magain, P. 1997, A&A, 328, 261
Nissen, P. E., Primas, F., Asplund, M., & Lambert, D. L. 2002, A&A, 390, 235
O'Neal, D., Saar, S. H., & Neff, J. E. 1996, ApJ, 463, 766
Ottmann, R., Pfeiffer, M. J., & Gehren, T. 1998, A&A, 338, 661
Peterson, R. C., Dalle Ore, C. M., & Kurucz, R. L. 1993, ApJ, 404, 333
Piskunov, N. E., Kupka, F., Ryabchikova, T. A., Weiss, W. W., & Jeffery, C. S. 1995, A&AS, 112, 525
Prochaska, J. X., Naumov, S. O., Carney, B. W., McWilliam, A., & Wolfe, A. M. 2000, AJ, 120, 2513
Randich, S., Gratton, R., & Pallavicini, R. 1993, A&A, 273, 194
Randich, S., Giampapa, M. S., & Pallavicini, R. 1994, A&A, 283, 893
Reddy, B. E., Tomkin, J., Lambert, D. L., & Allende Prieto, C. 2003, MNRAS, 340, 304
Ruland, F., Holweger, H., Griffin, R., Griffin, R., & Biehl, D. 1980, A&A, 92, 70
Saar, S. H., Nordström, B., & Andersen, J. 1990, A&A, 235, 291
Salasnich, B., Girardi, L., Weiss, A., & Chiosi, C. 2000, A&A, 361, 1023
Savanov, I. S., & Berdyugina, S. V. 1994, Astronomy Letters, 20, 227
Scheffler, H., & Elsässer, H. 1988, in Physics of the Galaxy and Interstellar Matter (Springer Verlag: Berlin)
Schlegel, D. J., Finkbeiner, D. P., & Davis, M. 1998, ApJ, 500, 525
Simmons, G. J., & Blackwell, D. E. 1982, A&A, 112, 209
Smith, V. V., Lambert, D. L., & Nissen, P. E. 1998, ApJ, 506, 405
Sneden, C. A. 1973, Ph.D. Thesis University of Texas, Austin
Soderblom, D. R. 1985, PASP, 97, 54
Solanki, S. K., & Unruh, Y. C. 1998, A&A, 329, 747
Soubiran, C. 1993, A&A, 274, 181

Table A.1. Continued.

λ (Å)	χ (eV)	log gf	EW (mÅ)[a]					
			UV For	VX Pyx	IN Vel	IS Vir	V764 Cen	V851 Cen
7751.137	4.992	–0.841	52.4		93.1	86.8		
7780.552	4.474	–0.175	127.5	168.9	173.4	164.1	208.2	144.4
7802.473	5.086	–1.493	23.0	45.4	47.8	40.5		
7807.952	4.992	–0.602	64.1	101.4	105.1	88.5		80.6
8922.643	4.992	–1.570	25.6					
Fe II; log $\epsilon_{\odot}$(Fe)=7.67								
5991.376	3.153	–3.702	29.1	62.3		39.0		26.5
6149.258	3.889	–2.858	26.3	65.9	48.2	51.8	54.4	35.4
6369.462	2.891	–4.192				32.4		
6416.919	3.892	–2.750	38.0	64.4		60.6	51.7	40.0
6456.383	3.904	–2.209	54.6	96.1	71.5	78.4		50.9
7711.723	3.904	–2.625	36.0	80.3	54.8	59.1	54.8	
Co I; log $\epsilon_{\odot}$(Co)=4.92								
6454.990	3.632	–0.233	33.6	48.6	57.4	47.2	65.1	32.7
Ni I; log $\epsilon_{\odot}$(Ni)=6.25								
5593.733	3.899	–0.683	51.5	75.7	83.3	68.2	86.5	61.3
5805.213	4.168	–0.530	45.3	69.5	70.2	63.2	62.8	52.8
6111.066	4.088	–0.785	38.4	71.3	70.0	61.0		52.0
6176.807	4.088	–0.148	72.4	98.5	101.1	88.5	124.9	77.2
6186.709	4.106	–0.777	43.6	68.4	75.1			
6204.600	4.088	–1.060	30.8	54.1	56.4	46.6	70.3	32.5
6223.981	4.106	–0.876	33.6	61.2		55.8		46.1
6772.313	3.658	–0.890	62.5	87.2	95.0	86.2	101.2	72.4
7555.598	3.848	0.069	105.9	142.1	144.6	131.2		112.4
7797.586	3.899	–0.144	89.1	121.8	122.4	118.7	147.2	105.2
Ba II; log $\epsilon_{\odot}$(Ba)=2.13								
5853.668	0.604	–0.758	92.8	132.4	142.2	151.5	165.0	119.9

[a] A blank indicates that the EW was not reliably measurable for one of the following reasons: the line was affected by telluric features or cosmetic defaults (e.g., cosmic rays), the line was significantly van der Walls broadened (see Sect. 4), or the Gaussian fit was judged unsatisfactory.

Strassmeier, K. G., Fekel, F. C., Bopp, B. W., Dempsey, R. C., & Henry, G. W. 1990, ApJS, 72, 191
Strassmeier, K. G., Hall, D. S., Fekel, F. C., & Scheck, M. 1993, A&AS, 100, 173
Strassmeier, K. G., Handler, G., Paunzen, E., & Rauth, M. 1994, A&A, 281, 855
Strassmeier, K. G., Washuettl, A., Granzer, Th., Scheck, M., & Weber, M. 2000, A&AS, 142, 275
Takeda, Y. 2003, A&A, 402, 343
Thévenin, F., & Idiard, T. P. 1999, ApJ, 521, 753
Unsöld, A. 1955, Physik der Sternatmospheren, MIT besonderer Berucksichtigung der Sonne (Berlin: Springer)
Vilhu, O., Gustafsson, B., & Edvardsson, B. 1987, ApJ, 320, 850
Yi, S., Demarque, P., Kim, Y.-C., et al. 2001, ApJS, 136, 417
Zahn, J.-P. 1994, A&A, 288, 829